OPTICAL BISTABILITY AND SOLITON SWITCHING IN AN OPTICAL RING CAVITY

by

Eric Curtis John Oliver

Thesis

submitted in partial fulfillment of the

requirements of the Degree of

Bachelor of Science with Honours in

Physics

Acadia University

April 2004

This thesis by Eric C. J. Oliver

is accepted in its present form by the

Department of Physics

as satisfying the thesis requirements for the degree of

Bachelor of Science with Honours

Approved by the Thesis Co-Supervisor

Dr. Holger Teismann	Date

Approved by the Thesis Co-Supervisor

Dr. Michael Robertson	Date

Approved by the Head of the Department

Dr. Bryan Latta	Date

Approved by the Honours Committee

	Date

I, Eric C. J. Oliver, hereby grant permission to the University Librarian at Acadia University to provide copies of the thesis, on request, on a non-profit basis.

_____

Signature of Author

_____

Date

Acknowledgements

I would like to thank Dr. Holger Teismann and Dr. Michael Robertson for their help and encouragement during the completion of this honours thesis. Thanks to Dr. Holger Teismann for his help with the mathematics, physical theory and numerical analysis. Thank you to the students and faculty of the Department of Physics at Acadia University as well as all of my friends and family for encouragement and interest in my honours work. I would like to thank the staff of the Vaughan Memorial Library for filling my endless requests for inter-library loans during my literature review. Finally, thank you to the Labrador Inuit Association for the financial support during the completion of my degree at Acadia University.

Contents

List of Figures

Abstract

This thesis presents the theory of the driven optical ring cavity containing a nonlinear material. First, an overview of the history of bistability and spatial solitons in driven nonlinear cavities is outlined. Then, the basic theory of the optical Kerr effect is presented and two of its consequences are outlined: optical bistability and spatial solitons. Within this background, the mirror feedback model is derived from the Maxwell-Bloch equations and considerations of the classical optics of the cavity. This model is analytically shown to exhibit bistability in the plane wave case. The mean-field model is subsequently derived by applying the mean-field limit to the Maxwell-Bloch equations and the cavity optics. In addition, the mean-field model is analytically shown to exhibit bistability in the plane wave case. Numerical simulations are performed on the mean-field model demonstrating the existence of: (i) plane wave bistability, (ii) transverse modulational bistability, (iii) the ability to "switch" between bistable states in both the plane wave and modulated case, (iv) instabilities in the modulated case and (v) the possibility for optimization of the switching process. Finally, an application of bistable driven cavities is explored: an all-optical digital information processor and storage device.

Chapter 1

Introduction to Nonlinear Optics and the Ring Cavity

Nonlinear optics is a field of physics that is rich with interesting phenomena. For many years the optical properties of materials were thought to be very well understood using the principles of classical optics. However, with the invention of the laser, the opportunity to probe matter with high intensity light has been made possible. Experiments with laser light and theories treating high intensity light-matter interactions has shown that the theories of classical optics do not give a complete description of such processes. Two examples of phenomena that occur because of the interaction of high intensity light with matter are optical bistability and spatial solitons.

Optical bistability occurs when an optical system exhibits two stable states for a single input value. Over the past two to three decades, bistability has been predicted for several optical systems including the optical ring and Fabry-Perot cavities and has recently been observed experimentally [1, 2, 3]. Optical spatial solitons are the spatial analogue to temporal solitons that are most commonly used in optical fibres and optical solitons in cavities have the potential to be used as optical bits for information

processing and storage. Experiments on driven optical cavities containing nonlinear materials have revealed the coexistence of bistability and spatial solitons where one of the two stable states of the system consists of solitons. In one such observation, the experimenters were able to switch the solitons on and off by shining a focussed beam of high intensity light into the nonlinear material [1].

In this thesis, the basic nonlinear processes that govern the mechanisms of optical bistability and spatial solitons will be outlined. The Maxwell-Bloch equations, the semi-classical dynamical equations that govern the interaction of light and matter, will be presented and applied to an optical ring cavity. From this starting point, two models for the optical ring cavity will be derived: the mirror feedback model and the mean-field model.

According to W. J. Firth and G. K. Harkness, the history of spatial solitons in optical cavities can be thought of as divided into three periods [4]. In the first period, there was little work being done on spatial structures in optical cavities except by a select few who have now become experts in the field. It was during this time period that the mirror feedback model was first developed by Maloney and his coworkers [5], which predicted the existence of bistability and spatial solitons. The second period began in the 1990s and was dominated by two areas of research: mean-field models and numerical simulations. The mean-field model of nonlinear optical cavities was a mathematical reduction of the mirror feedback model that predicted the existence of cavity solitons. The reduced nature of this model made it much more convenient to work with than the mirror feedback model. By the early 1990s, the power of computing facilities had reached a level such that numerical simulations of complex nonlinear problems could be performed with relative ease. Simulations performed on both the mirror feedback and mean-field models allowed scientists to probe the dynamical behaviour of such systems. The third period, which has been referred to as the "Information Age" [4], has just begun and holds much promise for future work

in this field. Experiments that demonstrate the existence of much that was predicted theoretically, including cavity solitons, are beginning to increase in numbers. In this ongoing period most theoretical work is being done on Fabry-Perot cavities containing semiconducting nonlinear materials [6, 7, 8]. Future work will highlight a movement from the theory of solitons in optical cavities to practical applications.

1.1 The Optical Kerr Effect

In the realm of nonlinear optics, there are many phenomena that arise due to a high intensity optical field (i.e.: laser light) being applied to a material. The optical Kerr effect occurs when a material's index of refraction is dependent on the intensity of this applied field and in principle, this effect can occur in all materials. There are several mechanisms that can give rise to the Kerr effect. An applied optical field can change the density of a material. In turn, this will change the electric susceptibility and the index of refraction. Another possibility is that the nonlinear terms in the electric susceptibility or refractive index are amplified by the applied field thus making their contribution significant with respect to the linear terms. In any case, the index of refraction, n, obeys the equation

$$n = n_0 + n_2' I \tag{1.1}$$

where I is the optical field intensity, n_0 is the linear refraction index and n_2' is a form of the optical Kerr coefficient (in units of m^2/W) which is typically on the order of 10^{-20} to 10^{-18} m^2/W in glasses, 10^{-18} to 10^{-11} m^2/W in doped glasses and 10^{-14} to 10^{-6} m^2/W in semiconductors [9]. An actual material will have higher order terms and so the Kerr effect is in fact a first order approximation. An optical material that exhibits this property is known as a Kerr medium. For our purposes, we will rewrite Eq. 1.1 as

$$n = n_0 + n_2 |E|^2 \tag{1.2}$$

since I is proportional to $|E|^2$. Here, the Kerr coefficient is in units of $\mathrm{m}^2/\mathrm{V}^2$ and since n_2 is small, the electric field, E, must be very intense for the Kerr effect to be significant. The Kerr effect is in fact an approximation for a general medium. The specific media that we will be considering is a two-level saturable absorber. The derivation of the electric susceptibility for such a material will be done in Sec. 2.1.2, however, for now it will be assumed to be of the form

$$\chi = \frac{\omega_{12} - \omega + i\gamma_{12}}{\gamma_{12}^2 + (\omega_{12} - \omega)^2 + \frac{4p^2}{\hbar^2}\frac{\gamma_{12}}{\gamma_{11}}|E|^2} \frac{p^2 n_1}{\epsilon_0 \hbar} = \frac{a + ib}{c + d|E|^2} \tag{1.3}$$

where $a = (\omega_{12} - \omega)\frac{p^2 n_1}{\epsilon_0 \hbar}$, $b = \gamma_{12}\frac{p^2 n_1}{\epsilon_0 \hbar}$, $c = \gamma_{12}^2 + (\omega_{12} - \omega)^2$, $d = \frac{4p^2}{\hbar^2}\frac{\gamma_{12}}{\gamma_{11}}$. Presently, the important characteristic is the nonlinear dependence of the susceptibility on the electric field. For a nonmagnetic material, we can relate the refractive index of a material to the relative permittivity, ϵ_r, by

$$n = \Re\left\{\sqrt{\epsilon_r}\right\}, \tag{1.4}$$

where $\Re$ denotes the real part, and the permittivity is related to the electric susceptibility by [10]

$$\epsilon_r = 1 + \chi. \tag{1.5}$$

By substituting in the susceptibility, taking the real part and Taylor expanding with respect to $|E|^2$, we get

$$n = \left(1 + \frac{a}{c} - \frac{ad}{c^2}|E|^2 + \cdots\right)^{\frac{1}{2}} \tag{1.6}$$

where $\cdots$ represents higher order terms. We can now perform a binomial expansion and also make the approximation that the higher order terms are small with respect

to the first two terms to get

$$n \simeq \left(1+\frac{a}{c}\right)^{\frac{1}{2}} - \frac{1}{2}\left(1+\frac{a}{c}\right)^{-\frac{1}{2}} \frac{ad}{c^2}|E|^2. \tag{1.7}$$

If we compare this approximation of the two-level saturable absorber index of refraction to the index of refraction from the Kerr effect, we can deduce the linear refractive index and the Kerr coefficient to be

$$\begin{aligned} n_0 &= \left(1+\frac{a}{c}\right)^{\frac{1}{2}} = \left(1+\frac{\omega_{12}-\omega}{\gamma_{12}^2+(\omega_{12}-\omega)^2}\frac{p^2 n_1}{\epsilon_0 \hbar}\right)^{\frac{1}{2}} & (1.8)\\ n_2 &= -\frac{1}{2}\left(1+\frac{a}{c}\right)^{-\frac{1}{2}} \frac{ad}{c^2} \\ &= -\frac{1}{2}\left(1+\frac{\omega_{12}-\omega}{\gamma_{12}^2+(\omega_{12}-\omega)^2}\frac{p^2 n_1}{\epsilon_0 \hbar}\right)^{-\frac{1}{2}} \frac{\omega_{12}-\omega}{\left(\gamma_{12}^2+(\omega_{12}-\omega)^2\right)^2}\frac{4p^4 n_1}{\epsilon_0 \hbar^3}\frac{\gamma_{12}}{\gamma_{11}}. & (1.9) \end{aligned}$$

It has been shown that the nonlinear effects of a saturable absorber lead to the Kerr effect, at least as a first-order approximation, and thus it is relevant to discuss the implications of the Kerr effect. Some of the phenomena that arise include: self-phase modulation, self-focussing, optical bistability and phase conjugate reflection [11]. The first two can lead to the existence of optical solitons if the optical field propagates in the presence of dispersion and diffraction, respectively. In the following sections, the properties of the Kerr effect that are relevant to this thesis will be discussed.

1.1.1 Optical Bistability

Optical bistability occurs when a cavity is filled with a Kerr medium and is pumped by a high intensity laser. Bistable operations have been predicted and observed in several optical systems since the 1960s [12] and other systems that exhibit optical bistability include pumped Pabry-Perot cavities and hybrid electro-optical bistable systems.

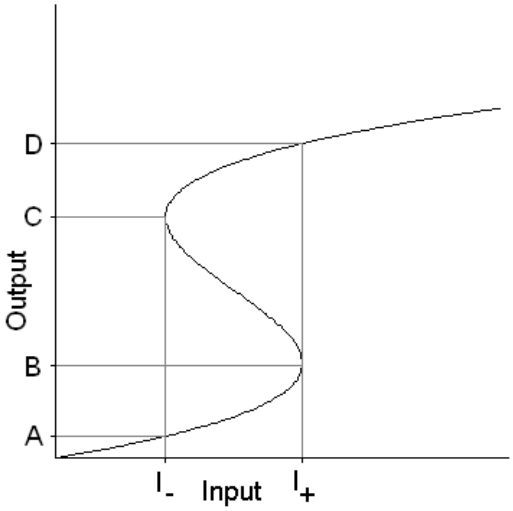

Figure 1.1: General Input-Output Bistability

Consider an physical system in which the output electric field versus the input electrical field can be described theoretically by the plot shown in Fig. 1.1. Imagine the system being driven by an input field below I_- so that the output field is below A. Now, the input is increased to I_+, and the output increases smoothly to B. Once the input is increased beyond I_+, the output suddenly jumps to D (in reality, "suddenly" is a finite time, dependent on the relaxation rates of the material [13]) and continues to increase above D. The point at which this jump occurs is known as the *switch-up point* and the level of high intensity output (from C to D and above) is called the *upper branch* of the bistability curve. If the state of the system lies on the upper branch beyond D and the input is decreased to I_-, the output decreases smoothly to C. As the input is decreased below I_-, the output "suddenly" jumps down to A and continues to decrease smoothly with the input. Similar to the *switch-up point*, this is known as the *switch-down point* and the level of low intensity output (from zero to B) is the *lower branch* of the bistability curve. It is known that the region of output lying between B and C is unstable [5] so this type of system has two stable output states lying between input fields of I_- and I_+ and its behaviour is labelled *bistability*.

The region between I_- and I_+ is called the *bistability region*. If the system is optical, as in the case of the ring cavity, then the system exhibits behaviour called *optical bistability*.

1.1.2 Self-Focussing and Self-Defocussing

Consider laser light with a Gaussian transverse intensity distribution propagating in a Kerr medium along the z-direction. For an increasing radius away from the beam centre, the index of refraction will change according to the intensity. If the Kerr coefficient n_2 is positive, the index of refraction decreases with the distance from the beam centre and effectively the medium acts like a focussing lens where the light beam is "compressed" towards its centre. Because the focussing is caused the by light itself, this phenomena is called *self-focussing* [9]. In the absence of diffraction, the light will continue to focus towards the centre of the material, increasing in intensity until damage to the material results. However, if the light is strongly diffracted, the focussing is countered by the diffractive spreading and if diffraction exactly counterbalances the self-focussing, then light is *self-trapping* and can be used as a simple explanation for the existence of *optical spatial solitons*. When n_2 is negative, the index of refraction increases with the distance from the beam centre and medium acts like a defocussing lens. This is called *self-defocussing* and under certain conditions the medium can support *dark* spatial optical solitons.

1.1.3 Spatial Optical Solitons

From a physical point of view, a soliton can be adequately described as a stable, localized state.[1] In optics, the state is an excitation of the optical field. The name "soliton" is derived from its defining properties. Solitons are localized, therefore can exist by themselves, and the first part of their name ("sol") refers to this solitary

[1] A more rigorous definition is used in mathematics, but this definition will be satisfactory for our purposes.

nature. Also, the stability of solitons is often analogous to that of a physical particle hence the "on" used in the second part of the name (i.e.: electron, proton, photon, etc.). Optical solitons are states of localized, stable, high intensity electric fields. Since intensity-dependent nonlinearities are necessary for optical solitons to form, these solitons are always of high intensity so that these nonlinearities play a significant role in the dynamics of the system. It will be shown in Sec. 4.4 that the upper branch of the bistability curve for the ring cavity consists of solitonic states.

Solitons occur in many different situations and in different forms. Mathematically, they appear as solutions to several equations including the nonlinear Korteweg-de Vries equation, the sine-Gordon equation and the nonlinear Schrödinger equation (a form of which we will be working with here). Solitons are particularly common among physical systems and have been predicted or observed in systems as diverse as water waves, optical fibres, quantum field theory and Bose-Einstein condensates.

As was described above, a simple explanation for the formation of solitons is that they are a balance of two forces: an outward force that works to expand the wave and an inward force that compresses the wave. For solitons in optical fibres, the compression is due to self-phase modulation (the temporal analogue of self-focussing) and the expansion is due to dispersion. These forces balance and can create a soliton that is localized in the time dimension as well as in the direction of propagation. As was mentioned above, diffraction can balance self-focussing and create a soliton that is localized in the space dimension that is transverse to the direction of light propagation.

1.1.4 Spatial Optical Solitons in Kerr Media

The existence of spatial optical solitons in Kerr media will be shown in the following section and this analysis is inspired by a similar undertaking presented in Ref. [14]. In that article, the derivation was performed by making an analogy to a mechanical

system and arguing that the solution for that system can be applied to the electromagnetic system. However, in the following analysis, only arguments using the principles of classical electromagnetism will be considered. The result will give us information on the properties of solitons that may exist in our system. As a starting point, we will use the wave equation for the electric field in a dielectric, nonmagnetic material:

$$\nabla^2 E = \frac{1}{v^2}\frac{\partial^2 E}{\partial t^2} \tag{1.10}$$

where v is the velocity of an electromagnetic wave in the material and can be expressed in the form:

$$v = \frac{c}{n} = \frac{c}{\sqrt{\epsilon_r}}. \tag{1.11}$$

From Sec. 1.1, we saw that we can can expand the nonlinear form of ϵ_r as

$$\epsilon_r = \epsilon_1 + \epsilon_2 |E|^2 \tag{1.12}$$

where, using the notation from Sec.1.1, $\epsilon_1 = 1 + \frac{a}{c}$ and $\epsilon_2 = -\frac{ad}{c^2}$. Here we have dropped terms of higher order than $|E|^2$, effectively making this a Kerr medium. We will consider a wave propagating in the z-direction with a transverse profile in the x-direction allowing us to reduce the Laplacian to $\nabla^2 = \frac{\partial^2}{\partial x^2} + \frac{\partial^2}{\partial z^2}$. We can substitute Eqs. 1.11 and 1.12 into Eq. 1.10 to get

$$\frac{\partial^2 E}{\partial x^2} + \frac{\partial^2 E}{\partial z^2} = \frac{\epsilon_1}{c^2}\frac{\partial^2 E}{\partial t^2} + \frac{\epsilon_2}{c^2}|E|^2\frac{\partial^2 E}{\partial t^2}. \tag{1.13}$$

For the type of wave described above, we can make the following ansatz:

$$E(x, z, t) = E(x)e^{i(\omega t - kz)}, \tag{1.14}$$

where taking the real part is implied. Substituting into Eq. 1.13 reduces the PDE wave equation to an ODE

$$\frac{d^2E(x)}{dx^2} - \kappa^2 E(x) + \epsilon_2 k_0^2 E^3(x) = 0 \tag{1.15}$$

where $k_0 = w/c$ and $\kappa^2 = k^2 - \epsilon_1 k_0^2$. If we integrate this equation over x once and rearrange the terms we obtain

$$\left(\frac{dE(x)}{dx}\right)^2 = \kappa^2 E^2(x) - \frac{1}{2}\epsilon_2 k_0^2 E^4(x). \tag{1.16}$$

The above expression can be rearranged with dx on the right-hand side and integrated from 0 to x

$$\int_{E(0)}^{E(x)} \frac{dE(x)}{\sqrt{\kappa^2 E^2(x) - \frac{1}{2}\epsilon_2 k_0^2 E^4(x)}} = \int_0^x dx \tag{1.17}$$

which can be rewritten as

$$\frac{1}{\kappa}\int_{E(0)}^{E(x)} d\left[\text{arcsech}\left(\sqrt{\frac{\epsilon_2}{2}}\frac{k_0}{\kappa}E(x)\right)\right] = \int_0^x dx \tag{1.18}$$

and the integrals evaluated, yielding

$$\frac{1}{\kappa}\left[\text{arcsech}\left(\sqrt{\frac{\epsilon_2}{2}}\frac{k_0}{\kappa}E(x)\right) - \text{arcsech}\left(\sqrt{\frac{\epsilon_2}{2}}\frac{k_0}{\kappa}E(0)\right)\right] = x. \tag{1.19}$$

Now, in order to proceed, we need to find the value of $E(0)$. We are looking for soliton solutions so we will make the assumption that the solution is localized in space about $x = 0$ and if we also assume that it is even, we can make the condition that $\left.\frac{dE(x)}{dx}\right|_{x=0} = 0$. By evaluating Eq. 1.16 at $x = 0$ and using this condition we get

$$E(0) = \sqrt{\frac{2}{\epsilon_2}}\frac{\kappa}{k_0}. \tag{1.20}$$

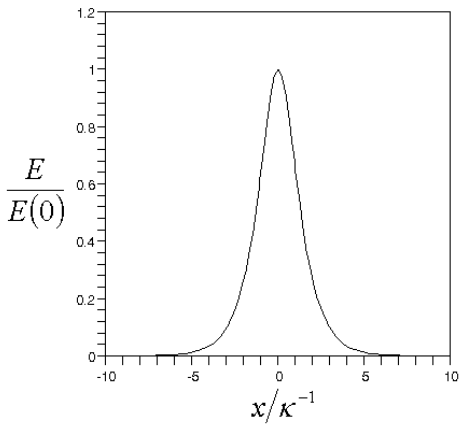

Figure 1.2: The Kerr Spatial Soliton

Substituting Eq. 1.20 into Eq. 1.19 and noting that arcsech(1) = 0, we can rearrange the equation and obtain the final solution:

$$E(x) = \sqrt{\frac{2}{\epsilon_2}}\frac{\kappa}{k_0}\text{sech}\left(\frac{x}{\kappa}\right). \tag{1.21}$$

Eq. 1.21 represents the transverse profile of one-dimensional electromagnetic soliton waves in Kerr media. As can be seen in Fig. 1.2, this solution is very localized in the x-direction. In order to preserve the generality of this argument x is scaled to κ^{-1} and E is scaled to $E(0)$ on the plot.

1.1.5 Soliton Solutions to the Nonlinear Schrödinger Equation

The differential equations that will become part of the mirror feedback and mean-field models of the ring cavity are forms of the nonlinear Schrödinger equation (NLS). The general mathematical form of this equation is

$$\frac{\partial u}{\partial t} - i\nabla^2 u = if(|u|^2)u \tag{1.22}$$

where u is complex and $f(|u|^2)$ is a function of $|u|^2$. The case where $f(|u|^2) = -1 + 2|u|^2$, also known as the cubic case, can be related to the Kerr nonlinearity and the case where $f(|u|^2) = \frac{-1}{1+2|u|^2}$ can be related to the saturable nonlinearity. An analytic mathematical technique known as Inverse Scattering can be used to solve this equation [9]. For the the cubic case there is a family of solutions in the form

$$u(x,t) = u_0 e^{it} \text{sech}(x - x_0). \tag{1.23}$$

This soliton solution to the NLS has much in common with the Kerr spatial soliton profile given in Eq. 1.21 and is localized in space around $x = x_0$. In Sec. 4.4.1, this type of solution will be used in the input field of the ring cavity system to try and force the cavity field it into a soliton state.

1.2 The Physical System: The Optical Ring Cavity

The physical system that will be analyzed for investigating optical bistability and soliton behaviour will be an optical ring cavity. Consider the system depicted in Fig. 1.3. A laser beam enters a cavity through a semipermeable mirror, M_1, with reflectance, R, and transmittance, T, where the transmittance and reflectance are related through the identity $R + T = 1$. Any effects due to absorption in the mirrors have been neglected. The cavity is partly filled with an optically nonlinear medium of length l_1 and the origin of the coordinate system is defined as the point where the light first enters the nonlinear medium. The light passes through the nonlinear medium and is redirected back to the entry point by a system of mirrors. The total length of the cavity is L, and the distance the light travels outside the nonlinear medium is l_2, where $l_1 + l_2 = L$. Two of the redirecting mirrors, M_3 and M_4, are assumed to be perfectly reflecting and the remaining mirror, M_2, has a reflectance and transmittance identical to M_1. By using this geometry, the state of the system

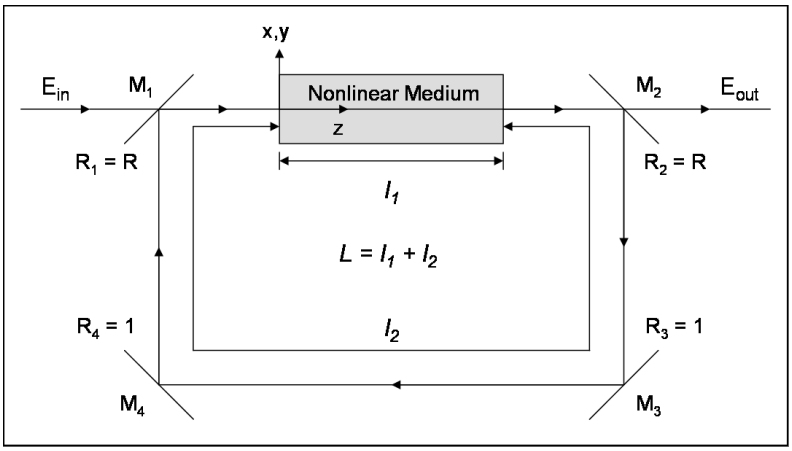

Figure 1.3: The Optical Ring Cavity

can be analyzed by measuring the light transmitted through M_2. The light in the cavity loses intensity with each reflection at M_1 and M_2 but this loss is compensated by continuous reinforcement provided by the input laser E_{in} at M_1. The aspect of the system that we would like to study is the behaviour of the electric field in the nonlinear medium after many cavity transits, or its steady state, and can be experimentally observed from the long term behaviour of E_{out}.

1.3 The Mathematical System: The Maxwell-Bloch Equations

The Maxwell-Bloch equations are a system of equations which govern the interaction of an electromagnetic wave with matter at the atomic level. They arise by combining the Maxwell equations for an electromagnetic wave with the Bloch equations for the dynamics of excited atoms in matter. The Bloch equations are derived from quantum mechanics, the Maxwell equations are from the classical theory of electromagnetism, thus the Maxwell-Bloch equations form a semi-classical approximation to the problem. In order to treat the interaction of electromagnetic waves and matter without approximation, the electric and magnetic fields would need to be quantized and we would analyze the relevant equations using quantum electrodynamics (QED). Since

the Maxwell-Bloch equations are a well established theoretical accomplishment, they will not be derived here.[2] Following the notation of Ref. [13] and assuming the non-linear medium to be a gas of two-level atoms, the Maxwell-Bloch equations can be expressed as

$$\frac{\partial A}{\partial z} + \frac{1}{c}\frac{\partial A}{\partial t} - i\frac{c}{2\omega}\nabla_{\perp}^{2}A + \frac{\kappa}{c}A = i\frac{\omega}{2\epsilon_0 c}\Lambda \tag{1.24}$$

$$\frac{\partial \Lambda}{\partial t} + (\gamma_{12} + i(\omega_{12} - \omega))\,\Lambda = i\frac{p^2}{\hbar}AN \tag{1.25}$$

$$\frac{\partial N}{\partial t} + \gamma_{11}(N - N_0) = i\frac{2}{\hbar}\left(A^*\Lambda - A\Lambda^*\right). \tag{1.26}$$

where $\nabla_{\perp}^{2} = \frac{\partial^2}{\partial x^2} + \frac{\partial^2}{\partial y^2}$. A is defined as the complex envelope of the electric field carrier wave, E, and Λ is the complex envelope of the polarization, P, (an asterisk denotes complex conjugates):

$$E(x,y,z,t) = A(x,y,z,t)e^{-i(\omega t - kz)} + A^*(x,y,z,t)e^{i(\omega t - kz)} \tag{1.27}$$

$$P(x,y,z,t) = \Lambda(x,y,z,t)e^{-i(\omega t - kz)} + \Lambda^*(x,y,z,t)e^{i(\omega t - kz)}, \tag{1.28}$$

where ω is the carrier wave (cw) frequency and k is the cw wavenumber. N is a real number giving the total difference in occupation probabilities between the two energy levels of the medium and a negative value for N quantifies the population inversion. The remaining terms are the speed of light, c, optical attenuation factor, κ, including properties of the material such as conductivity, free space permittivity, ϵ_0, and Plank's constant, $\hbar$. The electromagnetic field can induce dipole transitions in the nonlinear material and the strength of the transition is defined by p. The frequency difference between the ground (1) and excited (2) states, ω_{12}, is defined as $\omega_2 - \omega_1$, where $\omega_i = \epsilon_i/\hbar$ and ϵ_i is the energy of state i. The material decay and relaxation rates, γ_{ij}, are phenomenological terms for including quantum the effect of

[2] A thorough derivation of the Maxwell-Bloch equations used in this paper can be found in Ref. [13].

homogeneous broadening specifying the time taken for an energy state to decay due to irreversible losses that tend to push the system towards thermodynamic equilibrium. Such losses include effects from: particle collisons, phonon scattering and the fact that not all of the energy levels in the medium will be of exactly the same energy [5, 11, 13].

Chapter 2

The Mirror Feedback Model

The mirror feedback model of the optical ring cavity is the most straightforward of the two models that will be discussed. This model involves a reduction of the three Maxwell-Bloch equations to a single nonlinear partial differential equation for each pass through the cavity. This equation describes the time evolution of the electric field envelope in the nonlinear material and is coupled to a boundary condition that describes the free-space path of the light around the cavity. The derivation of this model is instructive in order to achieve some understanding of the dynamics of the optical ring cavity.

2.1 Derivation

The mirror feedback model has been previously derived in the literature [5, 13], however, the importance of re-deriving the model is to provide a consistent nomenclature and attempt to present it in a manner that follows the conventional notation of physics. First, classical optics will be used to account for electric field losses in the cavity. Second, the slowly varying envelope approximation will be made and allow the Maxwell-Bloch equations to be reduced to a single differential equation for the

electric field envelope. This final equation will hold for each individual pass of the ring cavity and the passes will be linked through the equation that describes the field losses.

2.1.1 Field Losses in the Ring Cavity

The boundary condition for the ring cavity will be derived considering the losses the electric field will undergo within the cavity and outside the nonlinear material. It will be quantified using classical optics. In order to formulate a simple boundary condition for the ring cavity, we will make the assumption that the diffraction of the electromagnetic wave in free space is negligible. Normally, this is not the case but the effect could be accomplished experimentally using a system of lenses to counteract the effects of diffraction. We will ignore the implications of such lenses in this model. Using the following optical definitions [15]:

$$E_{reflected} = \sqrt{R}E_{incident} \tag{2.1}$$

$$E_{transmitted} = \sqrt{T}E_{incident} \tag{2.2}$$

we can determine the change in electric field strength as the light travels around the free space portion of the cavity. During one complete transit of the ring cavity, the light is combined with the transmitted laser light at M_1. Therefore, the electric field strength will be increased by a value of $\sqrt{T}$ times the pumping electric field at that point, in accordance with Eq. 2.2. In addition, the electric field will be reduced by two identical partial reflections at M_2 and M_1 causing the field strength at the end of the nonlinear medium ($z = l_1$) to be reduced by a factor of $\sqrt{R}$ twice. However, in order for the state of the electric field to correspond to that of the previous pass, the time coordinate for this loss must be retarded by the time it took the light to travel the distance l_2. At a constant speed c, this time is l_2/c. If E is the electric field, the

losses in the cavity can be written mathematically as

$$E(x, y, 0, t) = \sqrt{T}E_{in}(x, y, 0, t) + RE(x, y, l_1, t - l_2/c) \tag{2.3}$$

Now, if we use Eq. 1.27 and assume the input beam is continuous (no z or t dependence), we can reduce Eq. 2.3 to

$$A(x, y, 0, t) = \sqrt{T}A_{in}(x, y) + Re^{ikL}A(x, y, l_1, t - l_2/c) \tag{2.4}$$

where $k = \omega/c$ is the wavenumber. From a physical point of view, it would make more sense to express $\exp(ikL)$ in terms of the cavity detuning angle, δ, where

$$\delta = \frac{\omega_c - \omega}{c}L. \tag{2.5}$$

This represents how far the incident frequency, ω, is detuned from the resonant cavity frequency, ω_c, and is useful since the characteristics of the electric field can be controlled by its frequency. From Appendix A, we can write $\exp(ikL)$ as $\exp(-i\delta)$ and the boundary condition becomes

$$A(x, y, 0, t) = \sqrt{T}A_{in}(x, y) + Re^{-i\delta}A(x, y, l_1, t - l_2/c). \tag{2.6}$$

2.1.2 The Evolution Equation for the Electric Field Envelope

We would like to reduce the complex, coupled Maxwell-Bloch equations to a single equation that will describe the behaviour of the electric field in the nonlinear medium. If attenuation of the optical wave is negligible, the fourth term in Eq. 1.24 can be ignored. Furthermore, if we make the slowly evolving envelope assumption that the field and atomic variables change slowly in the time over which the field envelope traverses the cavity (L/c), we can treat A, Λ and N as slowly varying functions of t within the confines of the nonlinear medium. However, once the field passes

through the medium and is redirected back to the beginning by the system of mirrors, it has undergone some losses so the slowly varying envelope approximation is no longer valid. This difficulty can be overcome by observing within each transit of the nonlinear medium, the fields are independent of t but require the boundary condition to supply their value for the next transit. This will allow us to make A, Λ and N time independent for each individual transit of the ring cavity, increasing the Maxwell-Bloch system from 3 equations to $3n$ equations:

$$\begin{aligned} \frac{\partial A_n}{\partial z} - i\frac{c}{2\omega}\nabla_\perp^2 A_n &= i\frac{\omega}{2\epsilon_0 c}\Lambda_n & (2.7)\\ (\gamma_{12} + i(\omega_{12} - \omega))\,\Lambda_n &= i\frac{p^2}{\hbar}A_n N_n & (2.8)\\ \gamma_{11}(N_n - N_0) &= i\frac{2}{\hbar}\left(A_n^*\Lambda_n - A_n\Lambda_n^*\right) & (2.9) \end{aligned}$$

where the subscript n corresponds to the nth transit of the cavity. However, this system can be simplified as follows. Solving Eq. 2.8 for Λ_n gives

$$\Lambda_n = \frac{1}{\gamma_{12} + i(\omega_{12} - \omega)}\frac{ip^2}{\hbar}A_n N_n. \tag{2.10}$$

Substituting this into Eq. 2.9 and leaving N_n implicit gives

$$N_n = \frac{-1}{\gamma_{12} + i(\omega_{12} - \omega)}\frac{2p^2}{\gamma_{11}\hbar^2}A_n A_n^* N_n - (\gamma_{12} + i(\omega_{12} + \omega))\frac{2}{\gamma_{11}p^2}\frac{\Lambda_n\Lambda_n^*}{N_n} + N_0. \tag{2.11}$$

For a complex quantity $z = x + iy$, we know that $zz^* = |z|^2 = x^2 + y^2$ and along with $|z_1/z_2|^2 = |z_1|^2/|z_2|^2$ and $|z_1 z_2|^2 = |z_1|^2|z_2|^2$, the value of $\Lambda_n\Lambda_n^*$ can be computed using Eq. 2.10

$$\begin{aligned} \Lambda_n\Lambda_n^* &= |\Lambda_n|^2 = \left|\frac{p^2}{\hbar}A_n N_n\left(\frac{i}{\gamma_{12} + i(\omega_{12} - \omega)}\right)\right|^2 \\ &= \frac{p^4}{\hbar^2}|A_n|^2 N_n^2\frac{|i|^2}{|\gamma_{12} + i(\omega_{12} - \omega)|^2} = \frac{p^4}{\hbar^2}|A_n|^2 N_n^2\frac{1}{\gamma_{12}^2 + (\omega_{12} - \omega)^2}. \quad (2.12) \end{aligned}$$

Substituting this into Eq. 2.11 we obtain

$$\begin{aligned} N_n &= \frac{-1}{\gamma_{12}+i(\omega_{12}-\omega)}\frac{2p^2}{\gamma_{11}\hbar^2}|A_n|^2N_n - \frac{\gamma_{12}+i(\omega_{12}+\omega)}{\gamma_{12}^2+(\omega_{12}-\omega)^2}\frac{2p^2}{\gamma_{11}\hbar^2}|A_n|^2N_n + N_0 \\ &= -\frac{2p^2}{\gamma_{11}\hbar^2}|A_n|^2N_n\left(\frac{1}{\gamma_{12}+i(\omega_{12}-\omega)} + \frac{\gamma_{12}+i(\omega_{12}+\omega)}{\gamma_{12}^2+(\omega_{12}-\omega)^2}\right) + N_0 \\ &= -\frac{2p^2}{\gamma_{11}\hbar^2}|A_n|^2N_n\left(\frac{2\gamma_{12}}{\gamma_{12}^2+(\omega_{12}-\omega)^2}\right) + N_0 \end{aligned} \tag{2.13}$$

and solving for N_n we get

$$N_n = \frac{N_0}{1+\frac{4p^2}{\hbar^2}\frac{\gamma_{12}}{\gamma_{11}}|A_n|^2\frac{1}{\gamma_{12}^2+(\omega_{12}-\omega)^2}}. \tag{2.14}$$

It will be assumed that all of the atoms in the nonlinear medium are initially in the ground state so that $N_0 = n_1$. This is an excellent approximation at low temperatures. Substituting this expression for N_n into Eq. 2.10 and then into Eq. 2.7 yields

$$\begin{aligned} \frac{\partial A_n}{\partial z} - i\frac{c}{2\omega}\nabla_\perp^2 A_n &= i\frac{\omega}{2\epsilon_0 c}\frac{1}{\gamma_{12}+i(\omega_{12}-\omega)}\frac{ip^2}{\hbar}A_n\frac{n_1}{1+\frac{4p^2}{\hbar^2}\frac{\gamma_{12}}{\gamma_{11}}|A_n|^2\frac{1}{\gamma_{12}^2+(\omega_{12}-\omega)^2}} \\ &= i\frac{\omega}{2c}\frac{p^2 n_1}{\epsilon_0\hbar}A_n\frac{i\left(\frac{\gamma_{12}^2+(\omega_{12}-\omega)^2}{\gamma_{12}+i(\omega_{12}-\omega)}\right)}{\gamma_{12}^2+(\omega_{12}-\omega)^2+\frac{4p^2}{\hbar^2}\frac{\gamma_{12}}{\gamma_{11}}|A_n|^2}. \end{aligned} \tag{2.15}$$

The complex numerator on the right hand side can be reduced by applying the algebraic rules of complex numbers. If we let $z = \gamma_{12} + i(\omega_{12} - \omega)$, the numerator becomes

$$\begin{aligned} i\left(\frac{\gamma_{12}^2+(\omega_{12}-\omega)^2}{\gamma_{12}+i(\omega_{12}-\omega)}\right) &= i\frac{|z|^2}{z} = i\frac{zz^*}{z} \\ &= iz^* = i(\gamma_{12} - i(\omega_{12}-\omega)) \\ &= \omega_{12} - \omega + i\gamma_{12}. \end{aligned} \tag{2.16}$$

Now, if we define the complex electric susceptibility to be

$$\chi(\omega, |A_n|^2) = \chi_R + i\chi_I = \frac{\omega_{12} - \omega + i\gamma_{12}}{\gamma_{12}^2 + (\omega_{12} - \omega)^2 + \frac{4p^2}{\hbar^2}\frac{\gamma_{12}}{\gamma_{11}}|A_n|^2} \frac{p^2 n_1}{\epsilon_0 \hbar} \tag{2.17}$$

then Λ_n is simply $\epsilon_0 \chi(\omega, |A_n|^2) A_n$ and the evolution equation for the electric field envelope $A_n(x, y, z, t)$ is

$$\frac{\partial A_n}{\partial z} - i\frac{c}{2\omega}\nabla_\perp^2 A_n = i\frac{\omega}{2c}\chi(\omega, |A_n|^2) A_n. \tag{2.18}$$

Thus, the original coupled Maxwell-Bloch equations have been reduced to n time independent differential equations for A that will describe the evolution of the electric field for each pass through the nonlinear medium along the longitudinal axis z and transverse axes x and y.

Now, all that is needed to solve this equation is to remove time from the boundary condition Eq. 2.6 and incorporate the idea of discrete cavity passes. The left hand side of the boundary condition corresponds to the initial data of the current (nth) pass and the field in the second term on the right hand side corresponds to the $z = l_1$ (i.e.: end of the material) data on the previous ($(n-1)$th) pass. Thus, we can dispense with the time variable as follows:

$$A_n(x, y, 0) = \sqrt{T} A_{in}(x, y) + Re^{-i\delta} A_{n-1}(x, y, l_1). \tag{2.19}$$

Using the transit number, n, instead of time, t, is preferable since it allows us to change the field equations to a set of n differential equations, each with its own boundary condition. The field equation system can now be solved by an iterative process. Given the initial data $A_1(x, y, 0)$, one can determine $A_1(x, y, l_1)$ from the differential evolution equation (Eq. 2.18). This value is substituted into the boundary condition (Eq. 2.19) to find $A_2(x, y, 0)$ and the process is iterated to determine the

behaviour of $A_n(x, y, l_1)$ for large n which corresponds to the steady state electric field in the nonlinear medium.

2.2 Plane Wave Steady State Case

In this section, we will consider the case where the input laser beam A_{in} does not depend on the transverse directions x and y (ie: it is a plane wave beam) and the cavity field is in a steady state. A plane wave steady state analysis is instructive in order to gain some knowledge about the general behaviour of the system and will be used as a benchmark when the mean-field approximation to this model is studied.

2.2.1 Plane Wave Input and Field Envelope

Since the pumping field is plane wave, A_{in} is simply a constant changing the boundary condition map given by Eq. 2.19 to

$$A_n(0) = \sqrt{T}A_{in} + Re^{-i\delta}A_{n-1}(l_1). \tag{2.20}$$

Note that the electric field envelope is now only a function of z and not of x or y. This is a direct consequence of the input being independent of x and y. If we consider the situation where $\omega_{12} - \omega$ is much greater than γ_{12}, the evolution PDE, Eq. 2.18, can be reduced to the ODE

$$\frac{dA_n}{dz} = i\frac{\omega}{2c}\chi_R(\omega, |A_n|^2)A_n. \tag{2.21}$$

Physically, this approximation means that the atomic detuning is a larger source of nonlinearity than homogeneous broadening. This in known as a *purely dispersive nonlinearity*. In addition, $|A_n|^2$ is constant in z as shown in Appendix B. This allows

for an analytic solution to Eq. 2.21

$$A_n(z) = A_n(0) \exp\left(i\frac{\omega}{2c}\chi_R(\omega, |A_n|^2)z\right) \tag{2.22}$$

which can be substituted into Eq. 2.20 to yield

$$A_n(0) = \sqrt{T}A_{in} + A_{n-1}(0)R \exp i\left(-\delta + \frac{\omega l_1}{2c}\chi_R(\omega, |A_{n-1}|^2)\right). \tag{2.23}$$

2.2.2 Plane Wave Bistability

We desire solutions that are asymptotically stable. That is, for large n, the map defined by Eq. 2.23 should leave $A_n(0)$ unchanged. These solutions are called fixed points of the map and can be found by taking the limit

$$\lim_{n\to\infty} A_n(0) = A(0), \tag{2.24}$$

thus changing our map to the nonanalytic equation

$$A(0) = \sqrt{T}A_{in} + A(0)Re^{i\phi} \tag{2.25}$$

where

$$\phi = -\delta + \frac{\omega l_1}{2c}\chi_R(\omega, |A|^2). \tag{2.26}$$

By rearranging, we can get the following equation and its complex conjugate:

$$1 - \frac{\sqrt{T}A_{in}}{A(0)} = Re^{i\phi} \tag{2.27}$$

$$1 - \frac{\sqrt{T}A_{in}}{A^*(0)} = Re^{-i\phi}. \tag{2.28}$$

By multiplying Eqs. 2.27 and 2.28 we get

$$\left(1-\frac{\sqrt{T}A_{in}}{A(0)}\right)\left(1-\frac{\sqrt{T}A_{in}}{A^*(0)}\right)=R^2 \tag{2.29}$$

and by adding Eqs. 2.27 and 2.28 and using the identity $e^{i\phi}=\cos\phi+i\sin\phi$ we obtain

$$2-\frac{\sqrt{T}A_{in}(A(0)+A^*(0))}{|A(0)|^2}=2R\cos\phi. \tag{2.30}$$

Solving Eq. 2.29 for $\sqrt{T}A_{in}(A(0)+A^*(0))$ (implicitly), substituting into Eq. 2.30, noting that $|A(0)|^2=|A_n|^2=|A|^2$ since $|A|^2$ is constant, and substituting in the value of ϕ, we derive the condition for the fixed points of the map given by Eq. 2.23

$$\cos\left(\frac{\omega l_1}{2c}\chi_R(\omega,|A|^2)-\delta\right)=\frac{1}{2}\left(\frac{1}{R}+R-\frac{TA_{in}^2}{R|A|^2}\right). \tag{2.31}$$

Eq. 2.31 gives the relation between the plane wave input field A_{in} and the field in the cavity. A plot of $|A|^2$ versus A_{in}^2 from Eq. 2.31 is presented in Fig. 2.1 where a change of variable has been made from A to F, the susceptibility is rewritten as reduced linear absorption, α_0, and material nonlinearity X.[1] The parameters were $l_1=2$, $R=0.9$, $\delta=0.4$, $\frac{\omega}{c}\frac{p^2n_1}{\epsilon_0\hbar\omega_{12}-\omega}=1$ and $\gamma_{12}\sqrt{\omega_{12}-\omega}=0.03$. One interesting aspect of this curve is that it exhibits a three-to-one correspondence between $|F|^2$ and F_{in}^2 within a well defined region. It is known that the central region is unstable [5] and in this region the system exhibits optical bistability as described in Sec. 1.1.1.

[1]Briefly and without explanation: $F=\frac{p}{\hbar}\sqrt{\frac{2}{\gamma_{11}\gamma_{12}}}$, $\chi=\frac{c}{\omega}\alpha_0 X$, $\alpha_0=\frac{\omega p^2 n_1}{\epsilon_0 c\hbar\gamma_{12}}$, $X=\frac{i+\Delta}{1+\Delta^2+2|F|^2}$ and $\Delta=\frac{\omega_{12}-\omega}{\gamma_{12}}$. See Appendix C for a more detailed discussion.

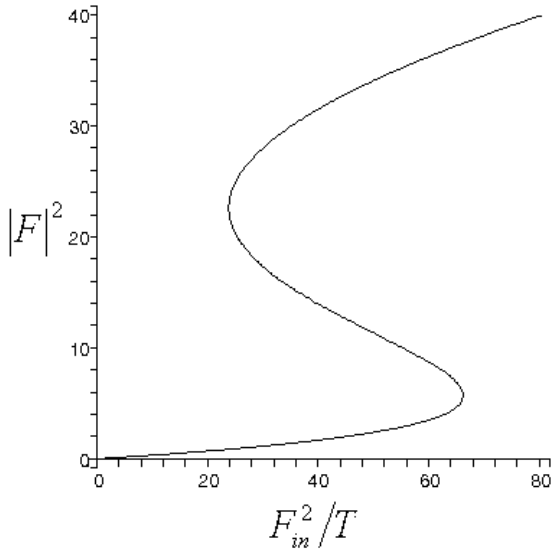

Figure 2.1: Bistability in the Mirror Feedback Model (Purely Dispersive Case)

Chapter 3

The Mean-Field Model

The mean-field model of the optical ring cavity is a reduction of the mirror feedback model. By taking mean-field limits and scaling the fields and coordinates, the mirror feedback model is reduced to a single partial differential equation with a periodic boundary condition.

3.1 Derivation

We begin the derivation of the mean-field model by considering the Maxwell-Bloch equations presented earlier as Eqs. 1.24 - 1.26

$$\frac{\partial A}{\partial z} + \frac{1}{c}\frac{\partial A}{\partial t} - i\frac{c}{2\omega}\nabla_{\perp}^{2} A = i\frac{\omega}{2\epsilon_0 c}\Lambda \tag{3.1}$$

$$\frac{\partial \Lambda}{\partial t} + (\gamma_{12} + i(\omega_{12} - \omega))\,\Lambda = i\frac{p^2}{\hbar} AN \tag{3.2}$$

$$\frac{\partial N}{\partial t} + \gamma_{11}(N - N_0) = i\frac{2}{\hbar}\left(A^*\Lambda - A\Lambda^*\right) \tag{3.3}$$

and with the ring cavity boundary condition also presented earlier as Eq. 2.6

$$A(x, y, 0, t) = \sqrt{T}A_{in}(x, y) + Re^{-i\delta}A(x, y, l_1, t - l_2/c). \tag{3.4}$$

It is possible to start the derivation of the mean-field model with the final equations of the mirror feedback model, but for completeness, we will use the full Maxwell-Bloch equations and the boundary condition above as our starting point.

3.1.1 The Mean-Field Limit

The mean-field approximation is an operation on the dynamical equations for the ring cavity that makes the cavity high finesse. A high finesse cavity is one in which there are very low losses and the mechanics of this approximation can be performed by taking the following limits [12, 16, 17, 18, 19]

$$T \to 0 \ \ (R \to 1) \ \ , \ \ \delta \to 0 \ \ , \ \ \alpha_0 l_1 \to 0 \tag{3.5}$$

where

$$\alpha_0 = \frac{\omega p^2 n_1}{\epsilon_0 c \hbar \gamma_{12}} \tag{3.6}$$

is derived from the linear absorption coefficient of the material (see Appendix C). These limits are performed so that the following quantities are kept constant:

$$\frac{\delta}{T} = \theta \ \ , \ \ \frac{\alpha_0 l_1}{2T} = C. \tag{3.7}$$

This is "mean-field" because the limit makes the cavity field approximately constant along the longitudinal cavity axis, z. The limit of transmittance to zero allows the field to undergo no loss from mirrors M_1 and M_2 and the limit of absorption to zero ensures that the field loses no intensity while travelling through the nonlinear material; essentially making the nonlinear medium infinitesimally thin. Finally, the limit of cavity detuning angle to zero guarantees that the field is tuned to perfect resonance within the cavity (i.e.: $\omega = \omega_c$). These limits are taken at certain rates so that the ratios in Eq. 3.7 remain constant ensuring that the field is constant along the cavity axis.

3.1.2 A Change of Variables

The first step in deriving the mean-field model is to make a change of variables motivated by the desire to simplify the boundary condition, Eq. 3.4. The independent variable for the time t is changed as $t \rightarrow t'$ where

$$t' = t + \frac{l_2}{c}\frac{z}{l_1}. \tag{3.8}$$

If this transformation is applied to the boundary condition Eq. 3.4, the BC becomes

$$A(x, y, 0, t) = \sqrt{T}A_{in} + Re^{-i\delta}A(x, y, l_1, t). \tag{3.9}$$

Next, there is a scaling of the electric field and polarization envelope variables:

$$\tilde{A}(x, y, z, t') = \exp\left(\frac{z}{l_1}(\ln R - i\delta)\right) A(x, y, z, t') \tag{3.10}$$

$$\tilde{\Lambda}(x, y, z, t') = \exp\left(\frac{z}{l_1}(\ln R - i\delta)\right) \Lambda(x, y, z, t'). \tag{3.11}$$

Note that under the mean-field limit, we get $\tilde{A} = A$ and $\tilde{\Lambda} = \Lambda$.

3.1.3 The Mean-Field Equations

In order to apply the field variable scaling to our equations and boundary conditions, we need to solve Eqs. 3.10 for A and 3.11 for Λ

$$A(x, y, z, t') = \exp\left(-\frac{z}{l_1}(\ln R - i\delta)\right) \tilde{A}(x, y, z, t') \tag{3.12}$$

$$\Lambda(x, y, z, t') = \exp\left(-\frac{z}{l_1}(\ln R - i\delta)\right) \tilde{\Lambda}(x, y, z, t') \tag{3.13}$$

as well as their complex conjugates

$$A^*(x,y,z,t') = \exp\left(-\frac{z}{l_1}(\ln R + i\delta)\right)\tilde{A}^*(x,y,z,t') \tag{3.14}$$

$$\Lambda^*(x,y,z,t') = \exp\left(-\frac{z}{l_1}(\ln R + i\delta)\right)\tilde{\Lambda}^*(x,y,z,t'). \tag{3.15}$$

The boundary condition Eq. 3.9 can now be simplified by substituting in Eq. 3.12, which yields

$$\tilde{A}(x,y,0,t) = \sqrt{T}A_{in} + R\exp(-i\delta)\exp(-\ln R + i\delta)\tilde{A}(x,y,l_1,t) \tag{3.16}$$

and reduces to the periodic boundary condition

$$\tilde{A}(x,y,0,t) = \sqrt{T}A_{in} + \tilde{A}(x,y,l_1,t). \tag{3.17}$$

Furthermore, under the mean-field limit (Eqs. 3.5), Eq. 3.17 reduces to

$$A(x,y,0,t) = A(x,y,l_1,t), \tag{3.18}$$

removing the need for an iterative process that was present in the mirror feedback model.

The Maxwell-Bloch equations must now be applied to the scaled field variables. First, the new polarization and population equations will be derived so that the steady state solutions can be used to simplify the electric field envelope equation before applying the mean-field limit. The polarization envelope equation can be found by substituting Eqs. 3.12 and 3.13 into Eq. 3.2 and cancelling the common exponential:

$$\frac{\partial\tilde{\Lambda}}{\partial t'} + (\gamma_{12} + i(\omega_{12} - \omega))\tilde{\Lambda} = i\frac{p^2}{\hbar}\tilde{A}N. \tag{3.19}$$

Under the mean-field limit we get

$$\frac{\partial \Lambda}{\partial t'} + (\gamma_{12} + i(\omega_{12} - \omega))\Lambda = i\frac{p^2}{\hbar} AN \tag{3.20}$$

which is identical to the original polarization equation (Eq. 3.2).

Obtaining the equation for the population N under the new variables is slightly more involved and we need to use the complex conjugates $\tilde{A}^*$ and $\tilde{\Lambda}^*$. Substituting Eqs. 3.12, 3.13, 3.14 and 3.15 into Eq. 3.3 and simplifying the exponentials gives

$$\frac{\partial N}{\partial t'} + \gamma_{11}(N - N_0) \;=\; i\frac{2}{\hbar} \exp\left(-2\frac{z}{l_1} \ln R\right) \left(\tilde{A}^* \tilde{\Lambda} - \tilde{A}\tilde{\Lambda}^*\right). \tag{3.21}$$

When the mean-field limit is applied to this equation, the exponential becomes unity and the terms with T go to zero leaving, as it was with the polarization envelope, an equation identical to the original

$$\frac{\partial N}{\partial t'} + \gamma_{11}(N - N_0) = i\frac{2}{\hbar}(A^*\Lambda - A\Lambda^*). \tag{3.22}$$

To solve for the variables relating to the material properties, Λ and N, we make the following approximation. From the material relaxation relaxation rates, γ_{11} and γ_{12}, we can calculate relaxation times $T_{11} = \gamma_{11}^{-1}$ and $T_{12} = \gamma_{12}^{-1}$. We will assume that these times are much smaller than the time over which the electric field varies. Therefore, the atomic variables respond very fast and quickly attain a steady state value. On the other hand, the electric field will still be varying in time after the atomic variables have reached equilibrium. We will only be considering the behaviour of the system over time scales that are much larger than T_{11} and T_{12} so we can ignore the time derivatives of Λ and N within the Maxwell-Bloch system and retain only the time derivative of the electric field envelope. This is known as the *good cavity approximation* [12]. It should be noted, should we want to consider the behaviour of

the Maxwell-Bloch equations over time scales on the order of, or smaller than, T_{11} and T_{12}, this approximation would not hold. Since Eqs. 3.20 and 3.22 are the same as the equations used in Sec. 2.1.2, they will yield the same steady state solutions. Therefore, we can simply quote the results derived earlier:

$$\Lambda = \epsilon_0 \chi(\omega, |A|^2) A = \frac{\omega_{12} - \omega + i\gamma_{12}}{\gamma_{12}^2 + (\omega_{12} - \omega)^2 + \frac{4p^2}{\hbar^2}\frac{\gamma_{12}}{\gamma_{11}}|A|^2} \frac{p^2 n_1}{\hbar} A. \tag{3.23}$$

We will now express χ in a simpler form by following the procedure outlined in Appendix C. This will introduce the material nonlinearity X as a function of the scaled field variable F. Performing this transformation will allow us to extract the reduced linear absorption coefficient α_0 for the mean-field limit:

$$\Lambda = \epsilon_0 \chi(\Delta, |F|^2) A = \frac{p^2 n_1}{\hbar \gamma_{12}} \frac{i + \Delta}{1 + \Delta^2 + 2|F|^2} A = \frac{p^2 n_1}{\hbar \gamma_{12}} X(\Delta, |F|^2) A. \tag{3.24}$$

The new electric field equation is found by substituting Eqs. 3.12, 3.13 and 3.24 into Eq. 3.1 and cancelling the common exponential, yielding

$$\frac{\partial \tilde{A}}{\partial z} + \frac{1}{c}\frac{\partial \tilde{A}}{\partial t'} - i\frac{c}{2\omega}\nabla_\perp^2 \tilde{A} = \frac{1}{l_1}(\ln R - i\delta)\tilde{A} + i\frac{\omega}{2\epsilon_0 c}\frac{p^2 n_1}{\hbar \gamma_{12}} X(\Delta, |F|^2)\tilde{A} \tag{3.25}$$

and we multiply this equation by c and factor $\frac{cT}{l_1}$ from the right side

$$c\frac{\partial \tilde{A}}{\partial z} + \frac{\partial \tilde{A}}{\partial t'} - i\frac{c^2}{2\omega}\nabla_\perp^2 \tilde{A} = \frac{cT}{l_1}\left(\frac{\ln R}{T}\tilde{A} - i\frac{\delta}{T}\tilde{A} + i\frac{\alpha_0 l_1}{T} X(\Delta, |F|^2)\tilde{A}\right). \tag{3.26}$$

Now, we can apply the mean-field limit. The limit of the term $\frac{\ln(R)}{T}$ is -1, which can be proven using L'Hopital's rule and $R = 1 - T$. We have assumed, from the mean-field limit, that the electric field envelope is uniform along the cavity axis, therefore we can now ignore the z derivative of the electric field. Also, in this step we will make the change of variables from A to F as defined in Appendix C. If we note that

the cavity linewidth is $\kappa = cT/l_1$, then the electric field envelope equation is

$$\frac{\partial F}{\partial t'} - i\frac{c^2}{2\omega}\nabla_\perp^2 F = \kappa\left(-F - i\theta F + i2CX(\Delta, |F|^2)F\right). \tag{3.27}$$

This equation has no source of pumping for the cavity. In order to facilitate such pumping we will add a pumping term *ad hoc*. This source will be analogous to A_{in} in the mirror feedback model. The new term is of the form κF_{in} and the final model equation is

$$\frac{\partial F}{\partial t'} - i\frac{c^2}{2\omega}\nabla_\perp^2 F = \kappa\left(F_{in} - F - i\theta F + i2CX(\Delta, |F|^2)F\right). \tag{3.28}$$

with the nonlinearity

$$X(\Delta, |F|^2) = \frac{i + \Delta}{1 + \Delta^2 + 2|F|^2}. \tag{3.29}$$

Eqs. 3.28 and 3.29 are known as the mean-field model for the optical ring cavity with a two-level atomic nonlinearity. This model is more desirable than the mirror feedback model from a mathematical analysis point of view as it reduces the complexity of the problem considerably. In the mirror feedback model, there was an identical differential equation for each complete circulation of the ring cavity by the electric field. In addition, there was also a boundary condition for each of these equations in the form of a single infinite dimensional map. Thus, the mirror feedback model had to be solved using an iterative process between the boundary conditions and the differential equations whereas the mean-field model reduces this complexity to a single differential equation and is much easier to analyze mathematically. However, this simplicity is achieved at the cost of many approximations and scaling of the electric field. There has been an analysis done in Ref. [20] comparing the two models, specifically the validity of the mean-field model. The conclusion of this paper was that the mean-field model can adequately describe the ring cavity provided there is only weak diffraction present.

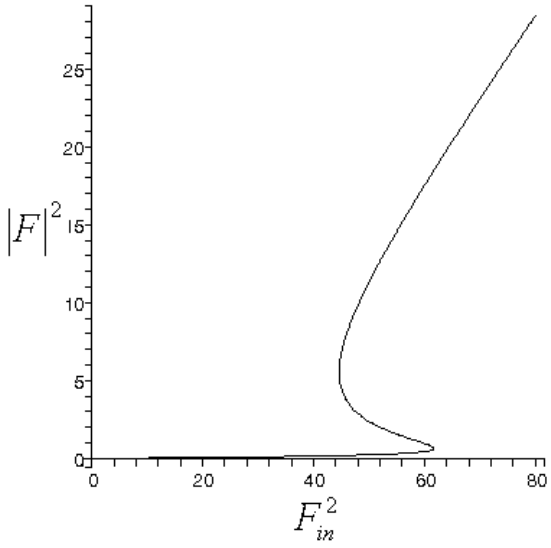

Figure 3.1: Bistability in the Mean-field Model (Resonant Case)

3.2 Plane Wave Steady State Case

In a similar manner to the mirror feedback model, we can investigate the plane wave case of the mean-field model at steady state. These steady state solutions are time-independent and spatially homogeneous in the transverse directions. If we make these two assumptions, the derivatives disappear in Eq. 3.28 and we get

$$F_{in} = \left(1 + i\theta + 2C\frac{1 - i\Delta}{1 + \Delta^2 + 2|F|^2}\right) F. \tag{3.30}$$

If the square of the modulus of Eq. 3.30 is taken

$$F_{in}^2 = |F|^2 \left[\left(\theta - \frac{2C\Delta}{1 + \Delta^2 + 2|F|^2}\right)^2 + \left(1 + \frac{2C}{1 + \Delta^2 + 2|F|^2}\right)^2\right]. \tag{3.31}$$

Eq. 3.31 represents the relationship between input field, F_{in}, and field in the medium, F, and is the analog of Eq. 2.31 from the mirror feedback model. Three cases can be considered. First, the frequency of the pumping beam is the same as the two-level transition frequency, ω_{12}, or $\Delta = 0$, and it is called the *resonant case*. Second,

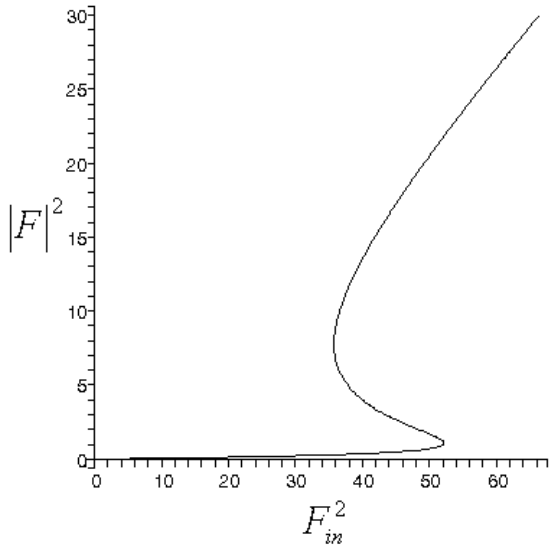

Figure 3.2: Bistability in the Mean-field Model (Focussing Case)

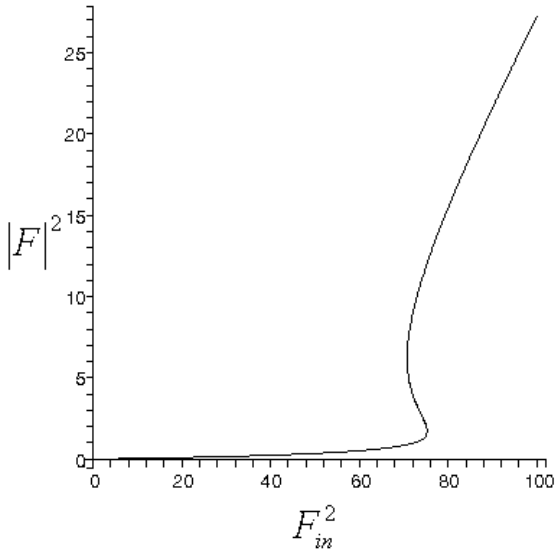

Figure 3.3: Bistability in the Mean-field Model (Defocussing Case)

the frequency is greater than the transition frequency. In this case, $\Delta < 0$ and the medium is said to be *focussing*. Third, the frequency is less than the transition frequency. In this case, $\Delta > 0$ and the medium is said to be *defocussing*. The last two cases refer to the focussing properties of a Kerr medium as described in Sec. 1.1.2. A plot of $|F|^2$ versus F_{in}^2 from Eq. 3.31 for each of these cases can be seen in Figs. 3.1 - 3.3 with parameters of $C = 10$ and $\theta = -1$. Analogous to the mirror feedback model, the mean-field model exhibits optical bistability as discussed in Sec. 1.1.1. The fact that bistability occurs in both models and for similar values of electric field is encouraging. This would lead one to believe that, at least as a very rough approximation, the mean-field model is an appropriate reduction of the mirror feedback model.

Chapter 4

Numerical Solutions

4.1 Numerical Methods

In order to examine the evolution of the electric field in the cavity after many cavity transits, we will move from analytic techniques to numerical methods. The computer software used to solve the system is called XMDS: eXtensible Multi-Dimensional Simulator [21]. The main benefit of XMDS is that it allows one to efficiently solve a physical problem that is described by a partial differential equation without needing to code complex programs and spending large amounts of time optimizing and debugging the algorithm. XMDS is a program that creates another program; it allows the user to specify a mathematical problem in XML (eXtensible Markup Language) code, a high-level language, and in turn writes a C program, a low-level language.

An example of the XML code for the mean-field equation can be found in Appendix D. The code specifies "RK4IP" as the integration algorithm which means that the differential equation is to be solved using the fourth-order Runge-Kutta method in the interaction picture. The fourth-order Runge-Kutta method has been a very successful method of solving both ordinary. The interaction picture is part of

a split-step method that evolves the field in both normal space and Fourier space in alternating steps [21].

4.2 Simulating the Mean-Field Equation

In order to facilitate numerical simulations several variables are rescaled. We will scale the time, transverse position and input field in Eq. 3.28 as follows [22]:

$$\tau = \kappa t' \quad , \quad (x', y') = \frac{(x, y)}{\frac{c^2}{2\omega}\kappa^{-1}} = \frac{(x, y)}{\frac{\lambda l_1}{4\pi T}}. \tag{4.1}$$

Noting that $\frac{c}{\omega} = \frac{1}{k} = \frac{2\pi}{\lambda}$ and $\kappa = \frac{cT}{l_1}$, simplifies the mean-field equation to give

$$\frac{\partial F}{\partial \tau} - i\nabla_\perp'^2 F = F_{in} - F - i\theta F + i2CX(\Delta, |F|^2)F, \tag{4.2}$$

where $\nabla_\perp'^2 = \frac{\partial^2}{\partial x'^2} + \frac{\partial^2}{\partial y'^2}$. It should be noted than on the axes of the plots on the following pages, τ appears as t and x' appears as x.

For the purposes of the numerical simulation, we have used a periodic boundary condition in x'. This is satisfactory providing the system is homogeneous in x' or that any localized structures are far from the boundary.

4.3 Switching Between Bistable States: Plane Wave Case

The bistability curve calculated in Sec. 3.2 assumed a solution that was independent of time and transverse spatial coordinates. Here we will attempt to reach plane wave steady states through a time evolved numerical simulation.

We will work with the scaled mean-field model as given by Eq. 4.2 and the plane wave case allows us to neglect the transverse Laplacian. We are looking for the steady state solutions and would like to try to reach these states through a time-dependent

pumping field. The bistability curves give the steady state solutions, but do not contain any information about reaching these states or about moving from one state to another in a time-dependent manner. F_{in} will be a function of time where its time-dependence is localized and the steady state solution determined to occur away from that point. Presently, we will only consider the case where the pumping field is tuned to atomic resonance. That is to say, $\Delta = 0$ in the nonlinearity $X(\Delta, |F|^2)$ term:

$$X(0, |F|^2) = \frac{i}{1 + 2|F|^2}. \tag{4.3}$$

Thus, the mean-field equation is now an ODE describing the time evolution of the system:

$$\frac{dF}{d\tau} = F_{in} - F - i\theta F - \frac{2C}{1 + 2|F|^2} F. \tag{4.4}$$

With respect to the control of the system, the parameter that is of interest is the input or pumping field, F_{in}. We would like to control the system so that the initial field is at a steady state on the upper or lower branch of the bistability curve and at some later time, t_0, it is "pushed" onto the other branch. This behaviour can be simulated by choosing the input field as:

$$|F_{in}(\tau)|^2 = H_0 + He^{-s(\tau-\tau_0)^2} \tag{4.5}$$

$$F_{in}(\tau) = \sqrt{H_0 + He^{-s(\tau-\tau_0)^2}} \tag{4.6}$$

where H, H_0, s and τ_0 are real constants. The second equation follows by assuming that the pumping field must be real, a reasonable assumption since F does not represent the field itself but rather the amplitude of the field envelope. For a time far from τ_0, we can make the approximation that $|F_{in}(\tau)|^2 \simeq H_0$ and H_0 is chosen such that the cavity field is at a steady state within the bistability region of the bistability curve. At $\tau = \tau_0$, the input field can be simplified to $|F_{in}(\tau)|^2 = H_0 + H$. The parameter H is chosen so that at $t = t_0$ the steady state cavity field is at a

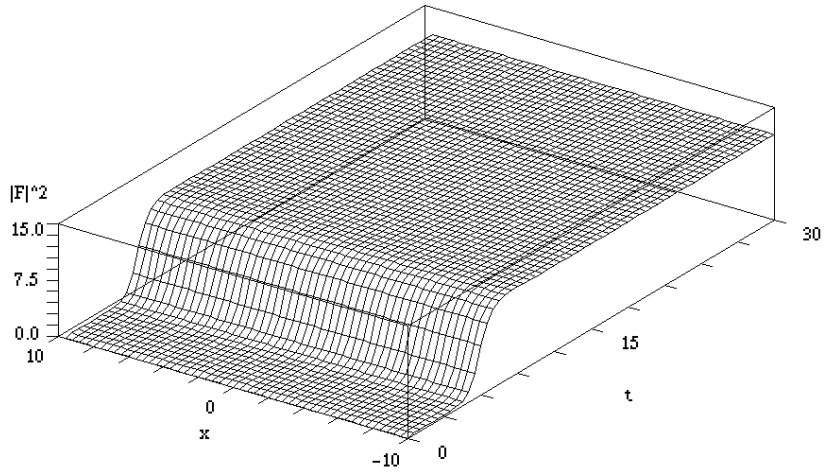

Figure 4.1: Plane Wave Switching On

point outside the bistability region either on the upper branch, if H is positive, or the lower branch, if H is negative. The time over which the *bump* of amplitude H is superimposed on H_0 is determined by the the *time-width*, s.

Consider the case where H is positive and the initial state of the system is on the lower branch of the bistability curve. For τ far below τ_0, the cavity is being driven at H_0 and the system reaches a steady state on the lower branch within the bistable region. As τ approaches τ_0, the pumping field approaches $H_0 + H$ which will drive the cavity field to the upper branch beyond the bistability region. For τ beyond τ_0, the pumping field relaxes back to H_0 and the system remains on the upper branch within the bistability region.

This creates a switching process. By applying the proper pumping field, the cavity field can be switched from a stable state of low intensity to a stable state of high intensity. In a similar fashion, if H is negative and the initial state of the system is on the upper branch, then the system can be switched down to a state of low intensity from a state of high intensity.

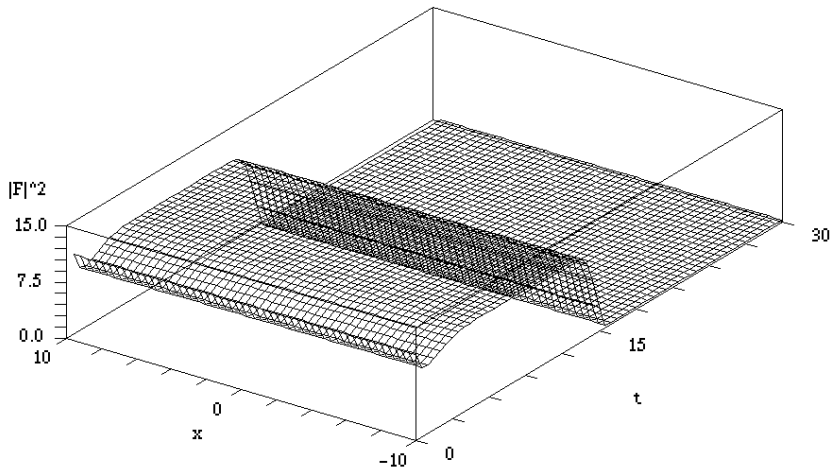

Figure 4.2: Plane Wave Switching Off

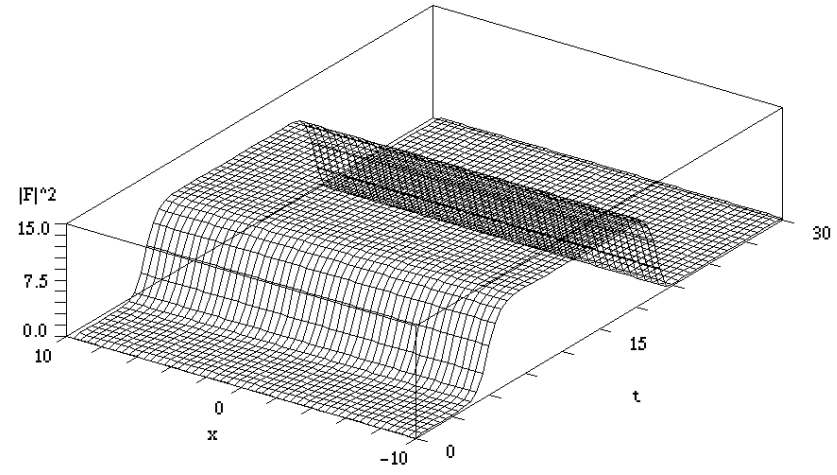

Figure 4.3: Plane Wave Switching On and Off

Examples of switching simulations performed using XMDS can be seen in Figs. 4.1 - 4.3. In all cases, the parameters are $C = 10$, $\theta = -1$ and $\Delta = 0$. In Fig. 4.1, the system is initially at $F = 0$ and is held on the lower branch with a pumping field of $H_0 = 50$ until $\tau_0 = 5$ where a bump of amplitude, $H = 25$, and time-width, $s = 1$, is superimposed. This bump switches the system onto the upper branch state where it remains after the bump has subsided. An example of switching off can be seen in Fig. 4.2 where the initial condition of the system is such that an input field of $H_0 = 50$ holds the system on the upper branch. At $\tau_0 = 5$, a bump of negative amplitude, $H = -25$, and time-width, $s = 1$, is superimposed on the pumping field and the system is switched to the lower branch. It is observed that the system requires a finite amount of time to settle in its steady state on the upper branch. This is because the initial condition for F is chosen with the both real and imaginary parts set equal. These values are chosen using the bistability curve such that the proper initial value of $|F|^2$ is obtained for the given H_0. However, the model equation is for F and the steady state may not have real and imaginary parts equal, yet still giving the same $|F|^2$. The short settling time is the system changing from the initial condition to its actual steady state field. The final plot in Fig. 4.3 shows the switching on and switching off mechanisms in sequence.

Thus, a method of switching the system between the upper and lower branches has been developed forming the basis of a one-bit logic system. The state represented by the upper branch state is the "on", or bit 1, and the lower branch is the "off", or bit 0. If we string multiple switch-on and switch-off methods together in a series we can create a series (in time) of on and off states or 0's and 1's.

4.4 Switching Between Bistable States: Modulated Case

If we could modulate the switching bump in the transverse dimension, it would be possible to create stable structures exhibiting localized properties that can be switched individually. The ability to switch multiple co-existing states on and off is more interesting and useful than the plane wave case since producing multiple states that can be switched creates a multi-bit system. We will make the claim that in the following modulated case, the upper branch of the bistability curve consists of solitonic states and this claim will be investigated by numerical simulation.

4.4.1 Switching a Single Soliton

Before attempting to create an array of solitonic states, the existence of a single state will the demonstrated. For now, we will consider the one-dimensional case where the only transverse dimension is x'. This means that the transverse Laplacian is simply $\nabla_{\perp}'^2 = \frac{\partial^2}{\partial x'^2}$ and the model equation is

$$\frac{\partial F}{\partial \tau} - i\frac{\partial^2 F}{\partial x'^2} = F_{in} - F - i\theta F + i2CX(\Delta, |F|^2)F. \tag{4.7}$$

As in the plane wave case, our controlling parameter is the pumping field, F_{in}, and taking the same form as Eq. 4.6 except that the time-dependent bump will be modulated by a localized function in the transverse dimension. Therefore, the form of the pumping field is chosen as

$$|F_{in}(\tau)|^2 = H_0 + H\text{sech}^2\left(w(x' - x_0')\right) e^{-s(\tau-\tau_0)^2} \tag{4.8}$$

$$F_{in}(\tau) = \sqrt{H_0 + H\text{sech}^2\left(w(x' - x_0')\right) e^{-s(\tau-\tau_0)^2}}. \tag{4.9}$$

In a similar manner to the plane wave case, we have a bump that is temporally localized and superimposed upon a constant background field. In addition, the bump

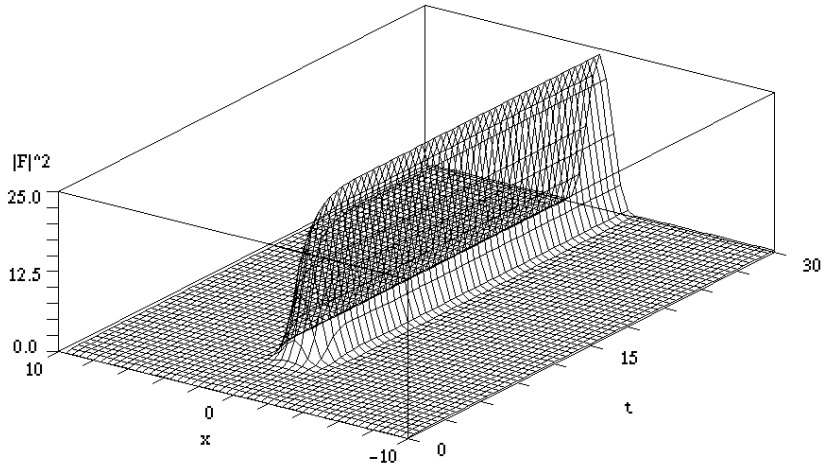

Figure 4.4: Switching a Soliton On

is now localized in space by the square of a hyperbolic secant function at $x' = x'_0$ with a width determined by w, called the *space-width*. The purpose of using the square of the hyperbolic secant is explained in Secs. 1.1.4 and 1.1.5. After conducting numerical simulations, a steady state solution is produced but is now shaped like a bump localized around $x' = x'_0$. We make the claim that these solutions are solitons. In the modulated case, it is observed that these solitons form the upper branch of the bistability curve.

If a bump of negative amplitude (a *dent*) is applied to a localized soliton state, the state will switch off in the same manner as the plane wave case. The amplitude of the applied dent must be large enough so that it forces the system down onto the lower branch of the bistability curve. In the modulated case, the lower branch still consists of plane wave states and so a switch down to the lower branch has the effect of switching the soliton off with only the plane wave background remaining.

Examples of soliton switching can be seen in Figs. 4.4 and 4.5. In these simulations, the PDE parameters were $C = 10$, $\theta = -1$ and $\Delta = 0$. The switching was

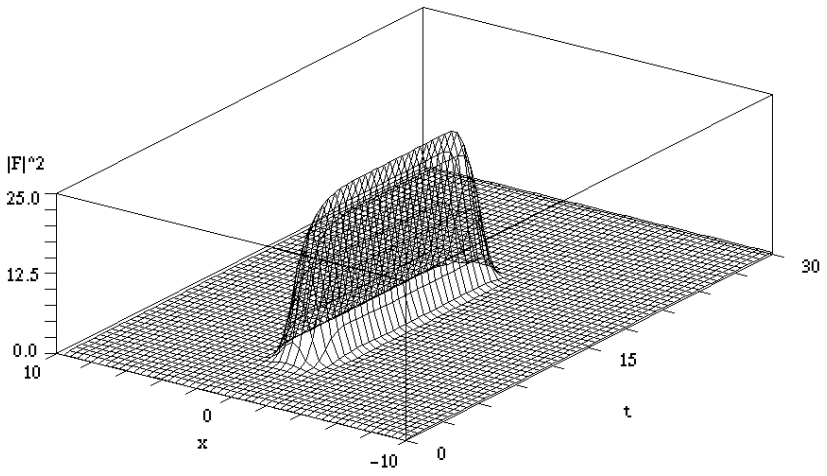

Figure 4.5: Switching a Soliton On and Off

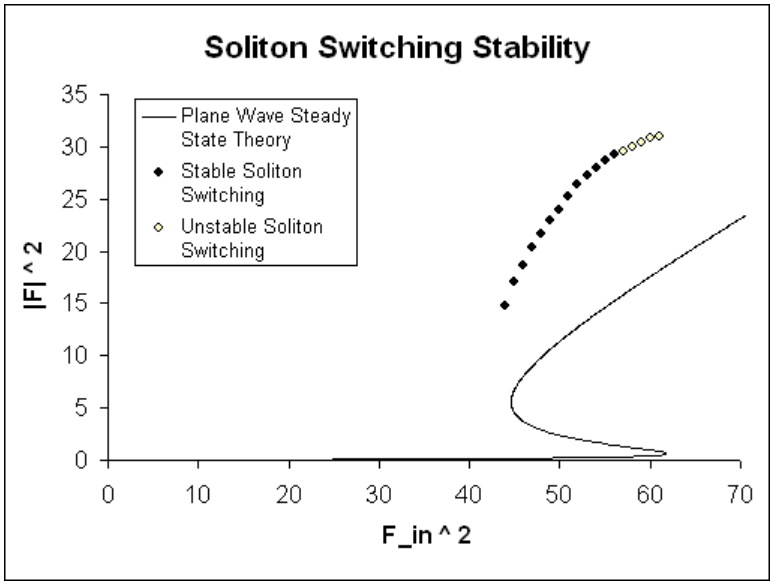

Figure 4.6: Stability Region of Soliton Switching (Resonant Case)

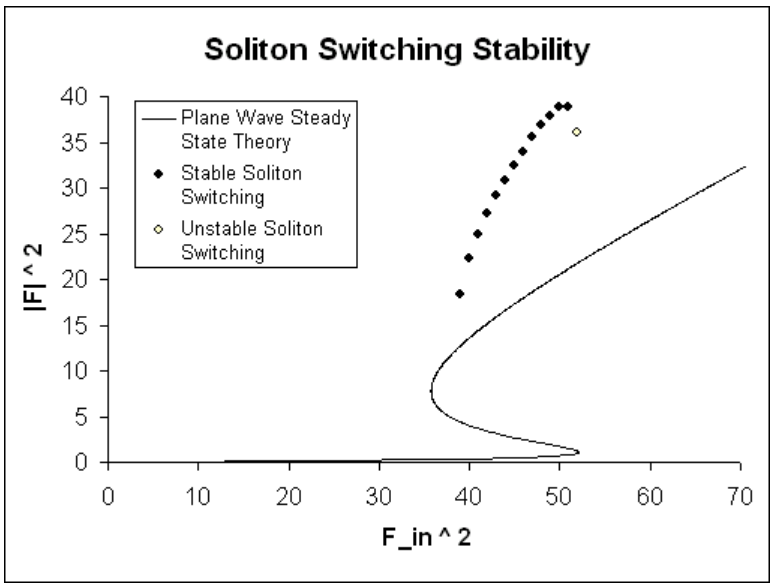

Figure 4.7: Stability Region of Soliton Switching (Focussing Case)

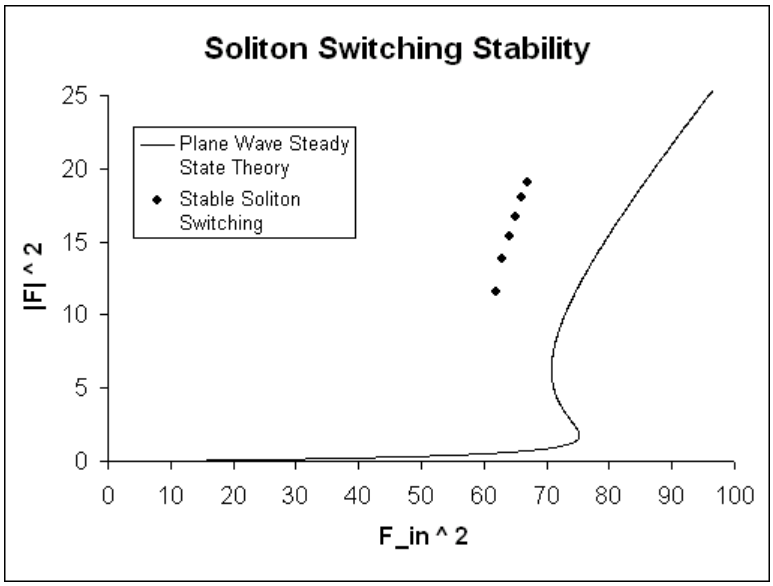

Figure 4.8: Stability Region of Soliton Switching (Defocussing Case)

performed with a bump of amplitude, $H = 40$, time-width, $s = 1$, and space-width, $w = 1$, superimposed on a plane wave background of $H_0 = 50$.

Unlike the regime of plane wave switching where all steady state solutions on the upper branch of the bistability curve are stable, this is not the situation with soliton switching. In the resonant case ($\Delta = 0$), only part of the upper branch represents a stable soliton solution with the remainder leading to unstable solutions. It can be seen in Fig. 4.6 that the upper branch contains both stable and unstable solutions. For a region starting from the beginning of the upper branch and increasing until a point within the bistability region, the solitons are stable. Above this point up to the end of the bistability region, the solitons are unstable. The nature of the instability can be explained as follows. In the unstable region a switching process will result in the creation of a soliton but the soliton quickly splits into two peaks that travel outwards in the x-direction at a constant velocity while maintaining a region of approximately constant, slightly lower intensity between the peaks. Once the peaks reach the boundary they decay and the cavity field reaches a plane wave steady state with an intensity the same as between the two unstable peaks. An example of this behaviour is given in Fig. 4.9. The behaviour of the instability settling down to a plane wave case may be a result of the periodic boundary condition. As can be seen in the numerical plot, the system does not settle down until it reaches the boundary. Nevertheless, this solution is an example of unstable soliton switching.

The same division of stable and unstable solitons exists in both the self-focussing case ($\Delta = -1$) and self-defocussing ($\Delta = 1$) cases. The modulated bistability curve for the focussing case is given in Fig. 4.7. The differences between this case and the resonant case are that a larger portion of the upper branch is stable and the upper branch begins at a larger F_{in}^2 than does the upper branch for the plane wave solutions. A qualitative explanation for the observation that the upper branch consists of more stable solutions than for the resonant case is that the medium is now self-focussing.

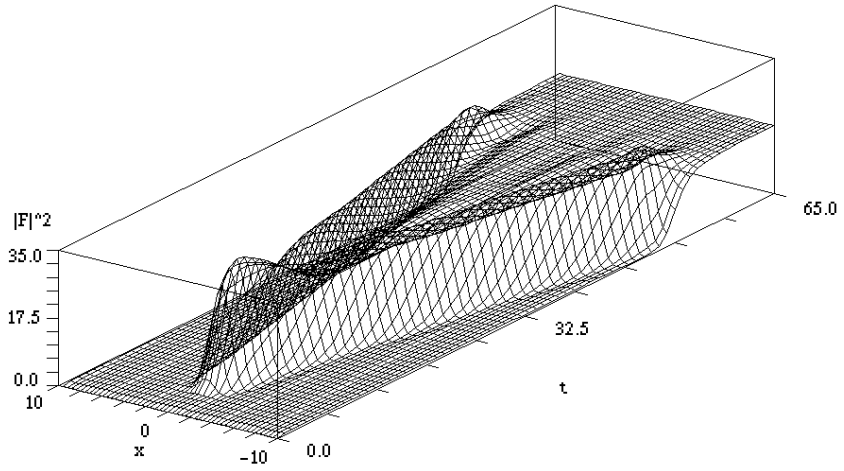

Figure 4.9: Unstable Soliton Switching (Resonant Case)

Since the nonlinearity of the medium is focussing and acting to support the existence of solitons, it is plausible that the medium can support these solitons for a wider range of parameters. In addition, for the self-focussing case the modulated upper branch has a region of negative slope at its upper end and this behaviour has been observed in other systems as well [4]. The self-defocussing case ($\Delta = 1$) supports solitons over a smaller portion of the upper branch than for the resonant and self-focussing cases and its bistability curve is given in Fig. 4.8. While the unstable solutions for the resonant and self-focussing cases possessed the same dynamics, the instability here is of a different nature. Shortly after forming a soliton, a pair of new solitons will form, one on each side of the first. After the formation of the new pair, another two will form, one on one side of the existing three and the second on the other side. This continues until the boundary is reached whereafter the multi-soliton solution becomes a steady state. This instability is displayed in Fig. 4.10. In a similar manner to the resonant and focussing instabilities, this steady state solution may be a product of the boundary conditions but is nonetheless an unstable soliton switch.

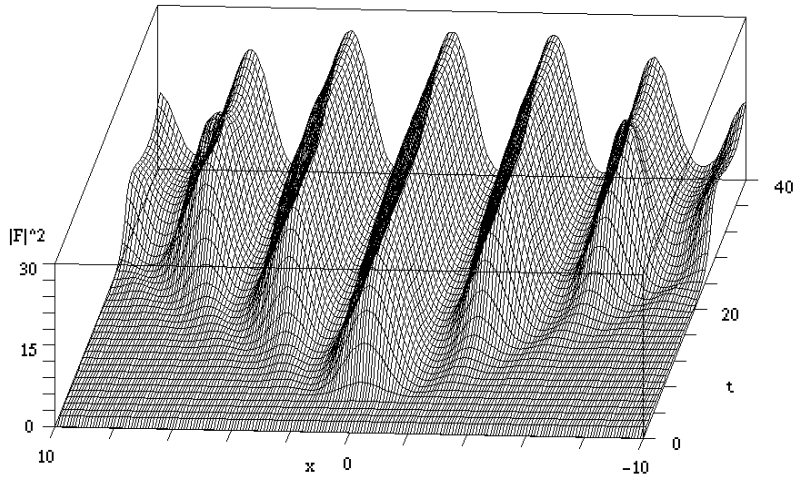

Figure 4.10: Unstable Soliton Switching (Defocussing Case)

4.4.2 Switching Multiple Solitons

Just as single solitons were switched on and off, we can also independently switch multiple solitons that coexist laterally in the x' dimension. The governing expression is still given by Eq. 4.7, however, the pumping field must be modified to include multiple soliton address pulses. For N solitons the pumping field is

$$|F_{in}(\tau)|^2 = H_0 + H \sum_{i=0}^{N} \operatorname{sech}^2 \left(w(x' - x'_i)\right) e^{-s(\tau-\tau_i)^2} \tag{4.10}$$

$$F_{in}(\tau) = \sqrt{H_0 + H \sum_{i=0}^{N} \operatorname{sech}^2 \left(w(x' - x'_i)\right) e^{-s(\tau-\tau_i)^2}}, \tag{4.11}$$

where x'_i and τ_i are the address position and time for the i^{th} soliton. There is no reason to assume that the individual solitons do not interact with one another and can be switched independently. However, the independent switching of three solitons can be observed in Fig. 4.11. In this simulation $i = 1, 2, 3$ with positions $x'_1 = 0$, $x'_2 = 5$, $x'_3 = -5$ and times $\tau'_1 = 5$, $x'_2 = 10$, $x'_3 = 20$. The switching bumps all have amplitudes, $H_0 = 50$, $H = 40$ as well as space-widths of $w = 1$ and a time-widths of

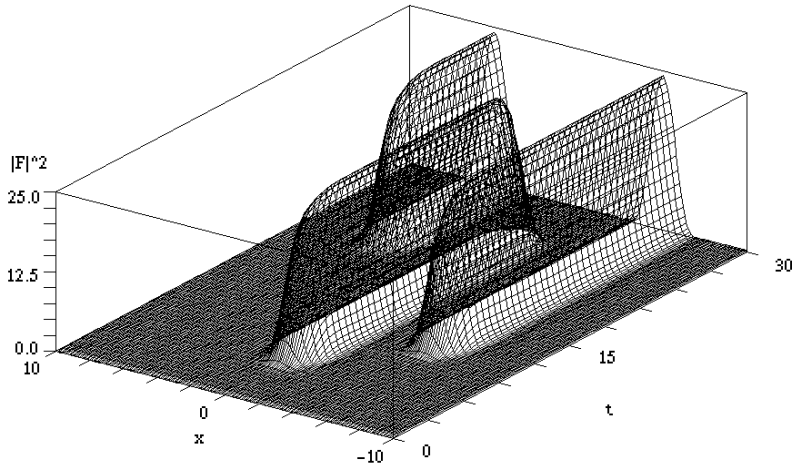

Figure 4.11: Switching Multiple Solitons

$s = 1$. There is also a switching-off bump applied at $x'_{1,off} = 0$ and $\tau'_{1,off} = 25$ with amplitude, $H = -40$.

It is observed that if two solitons are a sufficient distance from each other they can be treated independently. However, at closer distances the solitons do interact as can be seen in Fig. 4.12. In this simulation the distance between the switching bumps is $\Delta x' = 3.4$ and after the solitons are created they interact and finally merge a short time after. Since the cavity has a finite width in the x' dimension, we can only have a finite number of solitons existing before interactions with one another and the boundary result.

4.5 Optimizing the Switching Bump

In the interest of creating a practical device it is important to optimize the parameters that are relevant to the efficient operation of the device. It is apparent from the numerical results of both the plane wave and soliton switching examples that there is always a finite time for the switching between states to occur. This implies the

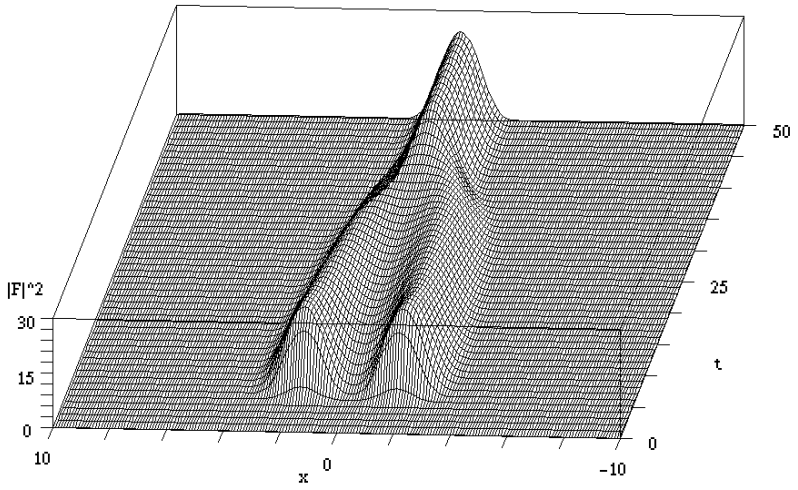

Figure 4.12: Multiple Solitons Merging

existence of a switching time, τ_s, that is a measure of the time between the application of the switching pump field and the time at which the cavity field stabilizes at a steady state.

If the time-width of the switching bump is too large, the system will require an excessive amount of time to switch states. An example of this behaviour can be observed in Fig. 4.13. The slow dynamics occur because the amplitude of the bump is varying so slowly that the relaxation rates of the material are fast enough to allow the cavity field to follow the applied field. In this simulation, the background and bump characteristics were the same as in Sec. 4.4.1 for the resonant case ($H_0 = 50$, $H = 40$, $w = 1$), however, here we have chosen $s = 5$ and it is apparent from the plot that the system follows the bump for a short time before it can switch to the upper state. On the other hand, if the bump is too narrow in time, the state will not switch at all. In this case, the amplitude of the bump varies too quickly for the material to react, and after the bump has subsided, the system has not had enough time to switch states.

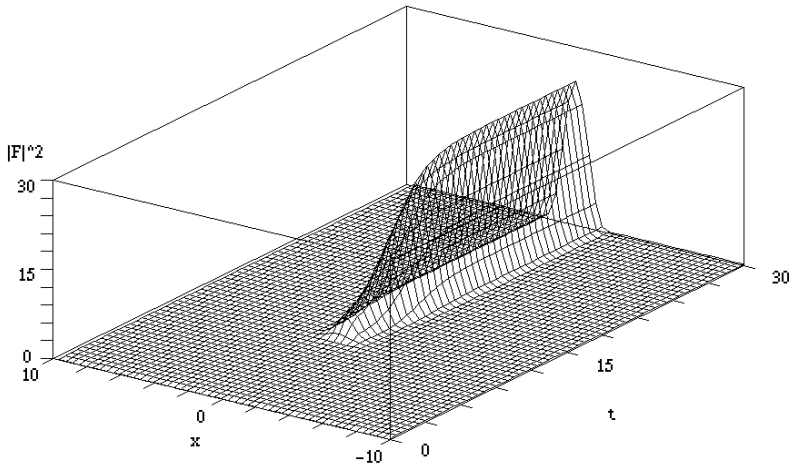

Figure 4.13: Inefficient (Slow) Soliton Switching

Chapter 5

Practical Applications

5.1 All-Optical Information Processor and Storage Device

The ability to switch multiple solitons on and off in an independent manner offers the possibility for use in an all-optical digital information processor. If we let the presence of a cavity soliton indicate the "1-bit" state and the absence of a cavity soliton the "0-bit" state, by proper control of the pumping field the operator can turn bits on and off at will. If this system is extended in the x-direction, the cavity could have sufficient space to create an N-bit system, thereby potentially creating the technology for all-optical digital information storage and processing system.

In addition to being switchable, the solitons in a ring cavity can be controlled by a suitable modulation of the pumping field. If the amplitude of the pumping field background is no longer constant but is a function of the transverse coordinate(s), the spatial distribution of the solitons can be controlled [23, 24]. Such an effect could also be created by modulating the phase of the pumping field because interference within the cavity field will translate the phase modulation into an amplitude modulation. In the presence of a pumping beam with a nonconstant background, a potential energy

field will be created that directly relates to this modulation. Under an amplitude modulation condition as described above, the local potential energy minima lie at local pumping field amplitude maxima. Therefore, solitons will be attracted to these amplitude peaks. If this potential could be varied in time, the solitons could be moved to a new position based on this controlled potential. This mechanism is not present in electrical systems and could prove useful in an all optical device.

Chapter 6

Conclusion

Optical spatial solitons in cavities have the possibility to revolutionize the way optical digital information is processed. The theory outlined in this thesis has demonstrated the features of an optical ring cavity containing a nonlinear material and driven by a high intensity laser. The mirror feedback model for this system has been derived and shown to exhibit optical bistability in a plane wave case, purely dispersive case. The mirror feedback model was reduced and approximated to the mean-field model, a more convenient form for evaluation, yet still exhibiting the same general characteristics as the mirror feedback model.

Numerical simulations of the mean-field model in one transverse dimension and time show that the mean-field model predicts both bistability and the existence of solitons as well as the intrinsic connection between the two effects. Plane wave bistability is present, as predicted from the theory. When the switching "bump" was modulated in the transverse dimension, it was shown that spatial solitons can be switched on and off. The connection between bistability and solitons is that these solitons represent the upper bistable state of the system under modulated conditions. In addition, the simulations were extended to show that multiple solitons can coexist

laterally and be switched independently, properties critical to the creation of all-optical switches. Lastly, factors affecting the the finite switching time between the "on" and "off" states were investigated.

The analysis presented in this thesis provides a solid background for application in two directions: the design of experiments and a theoretical analysis of similar systems. The numerical results presented in Chapter 4 would be useful for creating an experiment that would investigate the presence of solitons in a saturable nonlinear material. Also, there are several other systems currently being studied that are similar to the optical ring cavity, the most notable being a Fabry-Perot cavity containing a semiconducting nonlinear material [6, 7, 8]. The analysis presented in Chapters 2 and 3 could be extended to the geometries of Fabry-Perot systems and a numerical analysis similar to that presented in Chapter 4 could be performed. In conclusion, the optical ring cavity studied in this work has predicted useful nonlinear effects of optical bistability and switchable spatial solitons and has proven to be a very effective introduction into this rich subfield of nonlinear optics.

Appendices

A Cavity Detuning Angle δ

This appendix will define the cavity detuning angle δ. In the boundary condition given by Eq. 2.3 there is a term containing the expression $\exp(ikL)$. This expression can be expanded as $\exp(ikL) = \cos(kL) + i\sin(kL)$. Because of the periodic nature of the sine and cosine functions, this is equivalent to writing $\exp(i(kL - 2n\pi))$ where n is an integer.

The condition for resonance in an optical cavity is that the wavelength of the light be such that there is constructive interference over the length of the cavity. For this to occur, an integral number of wavelengths must exist within the length of the cavity, or, mathematically, $n\lambda_c = L$ where the subscript c denotes cavity resonance. This may, at first, appear to be contradictory to the resonance condition for a Fabry-Perot cavity which requires that $n\frac{\lambda_c}{2} = L$ for resonance to occur. However, in a Fabry-Perot cavity, there are two parallel mirrors separated by a distance L so that the light has to travel $2L$ in order to make a *complete* transit of the cavity. Therefore, if an integral number of half-wavelengths fits in the length L, an integral number of full wavelengths must fit in the entire cavity length $2L$, which is the resonance condition.

By definition, $\lambda_c = 2\pi/k_c$ and since $k = \omega/c$, this is equivalent to $\lambda_c = 2\pi c/\omega_c$. Substituting into the resonance condition we get

$$n\frac{2\pi c}{\omega_c} = L, \tag{A.1}$$

which can be rearranged as

$$2n\pi = \frac{\omega_c}{c}L. \tag{A.2}$$

Now, if this expression for $2n\pi$ is substituted into $\exp(ikL) = \exp(i(kL - 2n\pi))$ and using $k = \omega/c$ we get

$$\exp(ikL) = \exp\left(i\left(\frac{\omega}{c}L - \frac{\omega_c}{c}L\right)\right) \tag{A.3}$$

and defining the cavity detuning angle, δ, to be

$$\delta = \frac{\omega_c - \omega}{c}L \tag{A.4}$$

then Eq. A.3 can be reduced to

$$\exp(ikL) = \exp(-i\delta). \tag{A.5}$$

By using the relation given by Eq. A.5 the boundary in Sec. 2.1.1 can be simplified.

B Constant $|A|^2$

This appendix provides the details of the proof that $|A|^2$ is constant. Multiplying Eq. 2.21 by A^*

$$A^* \frac{dA}{dz} = i\frac{\omega}{2c}\chi_R(\omega, |A|^2)|A|^2 \tag{B.1}$$

where we have already noted the assumption for the plane wave case that $\chi \simeq \chi_R$. Differentiate $|A|^2$ with respect to z, which we want to be zero if $|A|^2$ is constant,

$$\begin{aligned}
\frac{d|A|^2}{dz} &= \frac{d(AA^*)}{dz} \\
&= A^*\frac{dA}{dz} + A\frac{dA^*}{dz} \\
&= A^*\frac{dA}{dz} + \left(A^*\frac{dA}{dz}\right)^* \\
&= 2\Re\left\{A^*\frac{dA}{dz}\right\}
\end{aligned} \tag{B.2}$$

where $\Re$ denotes the real part. If we substitute Eq. B.1 into the above expression we have

$$\frac{d|A|^2}{dz} = 2\Re\left(i\frac{\omega}{2c}\chi_R(\omega, |A|^2)|A|^2\right) \tag{B.3}$$

Since ω, c, χ_R and $|A|$ are all real, then this expression is zero thus $|A|^2$ is constant in z.

C Reduced Linear Absorption Coefficient α_0 and Material Nonlinearity X

Absorption is the loss of power as an electromagnetic wave propagates through a material. The absorption coefficient, α, is a measure of this loss in units of inverse distance and is defined by the following equation

$$E(z) = E(0) \exp\left(-\frac{\alpha}{2} z\right), \tag{C.1}$$

where E is the electric field strength.

For the ring cavity system, assuming a plane wave laser input, we have the following equation governing the behaviour of the electric field in the nonlinear medium

$$\frac{dA}{dz} = i\frac{\omega}{2c}\chi(\omega, |A|^2)A \tag{C.2}$$

which has the solution

$$A(z) = A(0) \exp\left(i\frac{\omega}{2c}\chi(\omega, |A|^2)z\right). \tag{C.3}$$

If χ is expanded into its real and imaginary parts and Eqs. C.1 and C.3 are compared, the absorption coefficient can be shown to be

$$\alpha = \frac{\omega}{c}\chi_I(\omega, |A|^2) = \frac{\omega}{c}\frac{p^2 n_1}{\epsilon_0 \hbar}\frac{\gamma_{12}}{\gamma_{12}^2 + (\omega_{12} - \omega)^2 + \frac{4p^2}{\hbar^2}\frac{\gamma_{12}}{\gamma_{11}}|A|^2} \tag{C.4}$$

where χ_I is the imaginary part of χ.

We would like to make the mathematics simpler for the derivation of the mirror feedback and mean-field models. To do this, we will define the reduced linear absorption coefficient, α_0, by altering the form of the complex electric susceptibility. First,

we will define a scaled form of the electric field envelope F

$$F = \frac{p}{\hbar}\sqrt{\frac{2}{\gamma_{11}\gamma_{12}}}A. \tag{C.5}$$

This scaling can be applied both to the field in the cavity as well as the input beam. If this new field variable is substituted into Eq. 2.17 for χ and both the numerator and denominator are divided by γ_{12}^2, χ can be reduced to

$$\chi(\Delta, |F|^2) = \frac{i + \Delta}{1 + \Delta^2 + 2|F|^2}\frac{p^2 n_1}{\epsilon_0 \hbar \gamma_{12}} \tag{C.6}$$

where $\Delta = \frac{\omega_{12}-\omega}{\gamma_{12}}$. Now if this definition of χ is substituted into Eq. C.4 we get

$$\alpha = \frac{\omega p^2 n_1}{\epsilon_0 c \hbar \gamma_{12}}\frac{1}{1 + \Delta^2 + 2|F|^2}. \tag{C.7}$$

We will now make two new definitions: the reduced linear absorption coefficient

$$\alpha_0 = \frac{\omega p^2 n_1}{\epsilon_0 c \hbar \gamma_{12}} \tag{C.8}$$

and the nonlinearity of the optical medium

$$X(\Delta, |F|^2) = \frac{i + \Delta}{1 + \Delta^2 + 2|F|^2} \tag{C.9}$$

such that

$$\alpha = \alpha_0 \Im\left\{X(\Delta, |F|^2)\right\}, \tag{C.10}$$

where $\Im$ denotes the imaginary part.

D XMDS Code

This appendix provides a sample of XML code used to create a C program from XMDS that will time-evolve the mean-field model. The code resembles the format of HTML for readers who are familiar with that format. I will briefly describe the significant portions of the code and a more detailed explanation of the basic format and notation can be found online at `www.xmds.org` under the documentation section.

The data within the <![CDATA[ ]]> braces is code that will be unchanged by XMDS and directly placed in the C program. The first set of code within these braces defines all of the constants (such as initial data, PDE parameters, etc.) to be used in solving the problem. The second section of C data defines the initial condition of the system. The third section of C data defines the transverse Laplacian in terms of an operator L. This operator acts like a second derivative on a plane wave function by replacing the derivitave by $-i(kx)^2/2$. The last C data set defines the differential equation. Note that F'_{in} must been written explicitly since it is dependent on the propagation dimension.

Under the <`field`> segment there are two specifications called `lattice` and `domains`. The `lattice` denotes the number of sample points to take in the transverse dimension and `domains` designates the range of values to sample over. Under the <`sequence`> <`integrate`> segment there are three specifications called `interval`, `lattice` and `samples`. The `interval` denotes the range of values in the propagation dimension over which the integration is performed and the `lattice` is the number of sample points that the range is divided into. The `samples` refer to the number of "snapshots" of the solution that are written to a data file. The resolution of the simulation will be greater with a larger lattice, however, the number of samples will only effect the resolution of the data set but not the accuracy of the simulation.

The code:

```
   <?xml version=‘‘1.0’’?>

<simulation>

   <prop_dim>t</prop_dim>
   <error_check>no</error_check>
   <stochastic>no</stochastic>

   <globals>
<![CDATA[
const double bump_dent_1 = 1;
const double t0_1 = 5;
const double x0_1 = 0;
const double s = 1;
// +1 is bump, -1 is dent,
// t0_i is time of bump/dent, x0_i is transverse position of bump/dent,
// s is time-width of bump/dent

const double w = 1;
const double H = 50;
const double A = 20; // H is height of plane wave,
// A is amplitude of bump/dent (both in units of |F|^2),
// w is space-width of bump/dent

const double IC = 0;
const double ic = sqrt(IC/2);
const double theta = -1;
const double Delta = 0;
const double C = 10;
// IC is initial state of system (in units of |F|^2),
// theta, Delta and C are PDE parameters

double sech(double);
double sech(double X)
{
return 1/cosh(X);
}
// defining the sech function
]]>
   </globals>

   <field>
      <name>main</name>
      <dimensions> x </dimensions>
      <lattice> 2000 </lattice>
      <domains> (-10,10) </domains>
```

```
      <samples> 1 </samples>
      <vector>
         <name>main</name>
         <type>complex</type>
         <components>F</components>
         <fourier_space>no</fourier_space>
<![CDATA[
F = complex(ic,ic);
// plane wave initial condition
]]>
      </vector>
   </field>

   <sequence>
      <integrate>
         <algorithm>RK4IP</algorithm>
         <interval> 150 </interval>
         <lattice> 1500 </lattice>
         <samples> 150 </samples>
         <k_operators>
            <constant>yes</constant>
            <operator_names>L</operator_names>
<![CDATA[
L = rcomplex(0,-kx*kx/2);
// this is the transverse laplacian in 1D
]]>
         </k_operators>
         <vectors>main</vectors>
<![CDATA[
dF_dt = L[F] + sqrt(H + bump_dent_1*A*exp(-s*pow(t-t0_1,2)) *
pow(sech(w*(x-x0_1)),2)) - F - i*theta*F + i*2*C*(i + Delta) /
(1 + pow(Delta,2) + 2*~F*F)*F;
// mean-field model.  Fin is here explicitly:  bump/dent localized
// in space and time with constant base height defined with H,
// bump/dent is initialized around t0,x0 with time-width s
// and space-width w.  ~F denotes complex conjugate.
]]>
      </integrate>
   </sequence>

   <output>
      <filename>mean-field_1D.xsil</filename>
      <group>
         <sampling>
            <fourier_space>no</fourier_space>
```

```
            <lattice> 50 </lattice>
            <moments>I</moments>
<![CDATA[
I=∼F*F;
// we are interested in is the intensity
// which is proportional to ∼F*F
]]>
          </sampling>
       </group>
   </output>

</simulation>
```

Bibliography

[1] Stephane Barland, Jorge R. Tredicce, Massimo Brambilla *et al.*, Nature **419**, 699 (2002).

[2] Carl O. Weiss, Gintas Slekys, Victor B. Taranenko, Kestutis Staliunas, and Robert Kuszelewicz. "Spatial Solitons in Resonators". *Spatial Solitons*. Ed. Stefano Trillo and William E. Torruellas. Springer-Verlag New York, Inc., New York: 2001.

[3] V. B. Taranenko, F.-J. Ahlers, and K. Pierz. arXiv:nlin.PS/0201013 v1 (2002).

[4] William J. Firth and Graeme K. Harkness. "Existence, Stability and Properties of Cavity Solitons". *Spatial Solitons*. Ed. Stefano Trillo and William E. Torruellas. Springer-Verlag New York, Inc., New York: 2001.

[5] H. Adachihara, D. W. McLaughlin, J. V. Maloney, and A. C. Newell, J. Math. Phys. **29**, 63 (1988).

[6] L. Spinelli, G. Tissoni, M. Brambilla, F. Prati, and L. A. Lugiato, Phys. Rev. A **58**, 2542 (1998).

[7] G. Tissoni, L. Spinelli, M. Brambilla, T. Maggipinto, I. M. Perrini, and L. A. Lugiato, J. Opt. Soc. Am. B **16**, 2083 (1999).

[8] G. Tissoni, L. Spinelli, M. Brambilla, T. Maggipinto, I. M. Perrini, and L. A. Lugiato, J. Opt. Soc. Am. B **16**, 2095 (1999).

[9] E. G. Sauter. *Nonlinear Optics*. John Wiley & Sons, Inc.: New York, 1996.

[10] Paul Lorrain, Dale R. Corson, and François Lorrain. *Electromagnetic Fields and Waves*. 3rd ed. W. H. Freeman and Company: New York, 1988.

[11] P. N. Butcher, and D. Cotter. *The Elements of Nonlinear Optics*. Cambridge University Press: Cambridge, 1990.

[12] L. A. Lugiato. "Optical Bistability". Vol. XXI, p. 69 of *Progress in Optics*. Ed. E. Wolf. North-Holland, Amsterdam: 1984.

[13] Alan C. Newell, and Jerome V. Maloney. *Nonlinear Optics*. Addison-Wesley Publishing Company: Redwood City, 1992.

[14] Raymond Y. Chiao. "Introduction to Spatial Solitons". *Spatial Solitons*. Ed. Stefano Trillo and William E. Torruellas. Springer-Verlag New York, Inc., New York: 2001.

[15] Frank L. Pedrotti, and Leno S. Pedrotti. *Introduction to Optics*. 2nd ed. Englewood Cliffs: Prentice-Hall, 1993.

[16] L. A. Lugiato, L. M. Narducci, E. V. Eschenazi, D. K. Brandy, and N. B. Abraham, Phys. Rev. A **32**, 1563 (1985).

[17] L. M. Narducci, and L. A. Lugiato, Phys. Rev. A **32**, 1576 (1985).

[18] L. M. Narducci, J. R. Tredicce, L. A. Lugiato, N. B. Brandy, and D. K. Brandy, Phys. Rev. A **32**, 1588 (1985).

[19] L. A. Lugiato, and C. Oldano, Phys. Rev. A **37**, 3896 (1988).

[20] M. Le Berre, D. Leduc, S. Patrascu, E. Ressayre, and A. Tallet, Chaos, Solitons and Fractals **10**, 627 (1999).

[21] *www.xmds.org*

[22] M. Brambilla, L. A. Lugiato, and M. Stefani, Europhys. Lett. **34**, 109 (1996).

[23] W. J. Firth, and A. J. Scroggie, Phys. Rev. Lett. **76**, 1623 (1996).

[24] G. S. McDonald, and W. J. Firth, J. Opt. Soc. Am. B **7**, 1328 (1990).